NAVAL POSTGRADUATE SCHOOL

MONTEREY, CALIFORNIA

THESIS

DIRECTION OF ARRIVAL DETERMINATION OF THE SOUND PRODUCED BY SMALL MULTI-ROTOR UAVS USING BIO-INSPIRED MEMS SENSORS

by

Jaemin Yang

September 2020

Thesis Advisor: Fabio D. Durante Pereira Alves
Co-Advisor: Gamani Karunasiri

THIS PAGE INTENTIONALLY LEFT BLANK

REPORT DOCUMENTATION PAGE	*Form Approved OMB No. 0704-0188*

1. AGENCY USE ONLY *(Leave blank)*	**2. REPORT DATE** September 2020	**3. REPORT TYPE AND DATES COVERED** Master's thesis

4. TITLE AND SUBTITLE DIRECTION OF ARRIVAL DETERMINATION OF THE SOUND PRODUCED BY SMALL MULTI-ROTOR UAVS USING BIO-INSPIRED MEMS SENSORS	**5. FUNDING NUMBERS**
6. AUTHOR(S) Jaemin Yang	
7. PERFORMING ORGANIZATION NAME(S) AND ADDRESS(ES) Naval Postgraduate School Monterey, CA 93943-5000	**8. PERFORMING ORGANIZATION REPORT NUMBER**
9. SPONSORING / MONITORING AGENCY NAME(S) AND ADDRESS(ES) N/A	**10. SPONSORING / MONITORING AGENCY REPORT NUMBER**

11. SUPPLEMENTARY NOTES The views expressed in this thesis are those of the author and do not reflect the official policy or position of the Department of Defense or the U.S. Government.

12a. DISTRIBUTION / AVAILABILITY STATEMENT Approved for public release. Distribution is unlimited.	**12b. DISTRIBUTION CODE** A

13. ABSTRACT (maximum 200 words)

In this study, the detection of the sound produced by multi-rotor small UAVs utilizing bio-inspired MEMS acoustic sensors is demonstrated. These sensors can be tuned by design to have the main resonance frequency matching the target spectral response. Different from conventional sensors, they are based on the hearing system of the parasitic fly *Ormia Ochracea* and can be operated at resonance. A multi-rotor small UAV acoustic signature is studied, and sensors designed specifically to detect a strong harmonic of the blade passing frequency are utilized to obtain the acoustic bearing. The MEMS sensors are arranged in canted angle configuration and the difference over the sum of their output voltages was found to be dependent on the angle of incidence. A simple algorithm with different integration times is applied and an unambiguous direction of arrival of the UAV sound is determined. All experiments were performed in anechoic chamber and the utilization of this method in open field is to be performed in future work. Results obtained without any calibration of signal processing show an average error and DOA determination about 11 degrees, which is better than what was obtained by complex microphone arrays, reported in the literature. These results indicate a great potential to use *Ormia*-based sensors for small UAV detection and localization.

14. SUBJECT TERMS MEMS, acoustic sensor, UAV, drone, detection, direction of arrival determination, DoA	**15. NUMBER OF PAGES** 69
	16. PRICE CODE

17. SECURITY CLASSIFICATION OF REPORT	**18. SECURITY CLASSIFICATION OF THIS PAGE**	**19. SECURITY CLASSIFICATION OF ABSTRACT**	**20. LIMITATION OF ABSTRACT**
Unclassified	Unclassified	Unclassified	UU

NSN 7540-01-280-5500 Standard Form 298 (Rev. 2-89) Prescribed by ANSI Std. 239-18

THIS PAGE INTENTIONALLY LEFT BLANK

Approved for public release. Distribution is unlimited.

DIRECTION OF ARRIVAL DETERMINATION OF THE SOUND PRODUCED BY SMALL MULTI-ROTOR UAVS USING BIO-INSPIRED MEMS SENSORS

Jaemin Yang
Lieutenant Commander, Republic of Korea Navy
BE, Naval Academy of Republic of Korea, 2008

Submitted in partial fulfillment of the
requirements for the degree of

MASTER OF SCIENCE IN ENGINEERING ACOUSTICS

from the

NAVAL POSTGRADUATE SCHOOL
September 2020

Approved by: Fabio D. Durante Pereira Alves
Advisor

Gamani Karunasiri
Co-Advisor

Oleg A. Godin
Chair, Department of Physics

THIS PAGE INTENTIONALLY LEFT BLANK

ABSTRACT

In this study, the detection of the sound produced by multi-rotor small UAVs utilizing bio-inspired MEMS acoustic sensors is demonstrated. These sensors can be tuned by design to have the main resonance frequency matching the target spectral response. Different from conventional sensors, they are based on the hearing system of the parasitic fly *Ormia Ochracea* and can be operated at resonance. A multi-rotor small UAV acoustic signature is studied, and sensors designed specifically to detect a strong harmonic of the blade passing frequency are utilized to obtain the acoustic bearing. The MEMS sensors are arranged in canted angle configuration and the difference over the sum of their output voltages was found to be dependent on the angle of incidence. A simple algorithm with different integration times is applied and an unambiguous direction of arrival of the UAV sound is determined. All experiments were performed in anechoic chamber and the utilization of this method in open field is to be performed in future work. Results obtained without any calibration of signal processing show an average error and DOA determination about 11 degrees, which is better than what was obtained by complex microphone arrays, reported in the literature. These results indicate a great potential to use *Ormia*-based sensors for small UAV detection and localization.

THIS PAGE INTENTIONALLY LEFT BLANK

TABLE OF CONTENTS

THIS PAGE INTENTIONALLY LEFT BLANK

LIST OF FIGURES

LIST OF ACRONYMS AND ABBREVIATIONS

BPF	Blade Passing Frequency
DAS	Data Acquisition System
DoA	Direction of Arrival
FAA	Federal Aviation Administration
FWHM	Full Width at Half Maxima
IR	Infrared
IWM	Incoherent Wideband Music
MEMS	Micro electrical mechanical systems
NPS	Naval Postgraduate School
PCB	Printed Circuit Board
RF	Radio Frequency
SEM	Scanning Electron Microscope
SOIMUMPS	Silicon-on-insulator multi-user manufacturing process
SPL	Sound Pressure Level
TFDSB	Frequency Delay and Sum Beaming
UAV	Unmanned Aerial Vehicle
V	Voltage
VTOL	Vertical Take-Off and Landing

THIS PAGE INTENTIONALLY LEFT BLANK

EXECUTIVE SUMMARY

Currently, small unmanned aerial vehicles (UAV) are used in many fields, including shipping, delivery, architecture for creating topographic surveys, photography, search and rescue, security and defense among many others. The technology has enabled a tremendous reduction in cost; therefore, the number of small UAVs is expected to continue rising as their applications are expanding.

In the same way that small, multi-rotor UAVs can be explored as great assets in the defense realm, they also pose a considerable threat to military operations. Many efforts have been conducted to prevent UAVs from performing surveillance, terrorist, or military attacks. Potential countermeasures cannot be employed, however, if the threat is not detected.

Recent studies have sought to develop small UAV-detection systems using radar, electro-optics (i.e., cameras, infrared (IR)), acoustics, and radio frequency [1]. Each method has its own specific limitations; one that is common to all, however, is the difficulty of detecting smaller targets. An approach that is independent of the size of the aircrafts is acoustic detection that targets the sound emitted by the aircraft's rotors. Furthermore, acoustic detection is a passive process, which can be important in defense applications. Although many acoustic systems have been proposed for detection of small UAVs, the proposed systems share at least one common characteristic, the use of conventional microphones, which suffers from detection range limitations and requires complex array arrangements for localization of the source.

Researchers from the Sensor Research Laboratory have been investigating an approach to detect the presence and the direction of small UAVs using microelectromechanical systems (MEMS) directional acoustic sensors, based on the anatomical structure of the ears of the parasitic fly *Ormia Ochracea* [2]. These sensors have proved to be very efficient in providing unambiguous directional detection of single-tone acoustic sources and blast sounds such as bomb explosions and gunshots [3]. Building on this success, ***the objective of this thesis is to demonstrate the ability to detect***

the bearing of a small UAV using colocated, canted, Ormia-based MEMS sensors. These sensors have the advantage of possessing directional accuracy [3], a very small form factor, and low power consumption—even with the inclusion of the amplification electronics.

To prove the concept just described, the study reported in this thesis relies on the similarities between acoustic signatures of small multi-rotor UAVs [4], [5], and concentrates on the general characteristics of the sound generated by a particular small hexacopter (Yuneek Typhoon) in hovering regime. Based on these characteristics, an *Ormia*-based MEMS acoustic directional sensor was designed to exhibit resonant response around 700 Hz, to match the strong emission of the source. One advantage of operating at resonance while having a reasonable quality factor is the ability to naturally filter out a large portion of undesirable background noise.

Several MEMS sensors were characterized, and a pair with matching frequency response was selected and mounted with a canted angle of 15 degrees. The sound of the Typhoon was played in an anechoic chamber while the sensor was rotated. The data from both sensors was recorded and a simple algorithm applied to compute the direction of arrival. The results show reasonable agreement between the actual and measured angle of arrival. Figure 1 shows this comparison where the ideal detector (actual angle) is represented by the solid straight line and the estimated angle based on the measurements is indicated by the circular markers. The results show that the error between the measured and actual angle of arrival is up to 20 degrees, with an average of 11 degrees, which is very encouraging: No signal conditioning such as filtering, rectification, smoothing, etc., or signal processing other than integration was applied. It is observable that there is no ambiguity in the range of detection, and with the application of simple calibration methods such as fitting curves or lookup tables, accuracy can greatly increase.

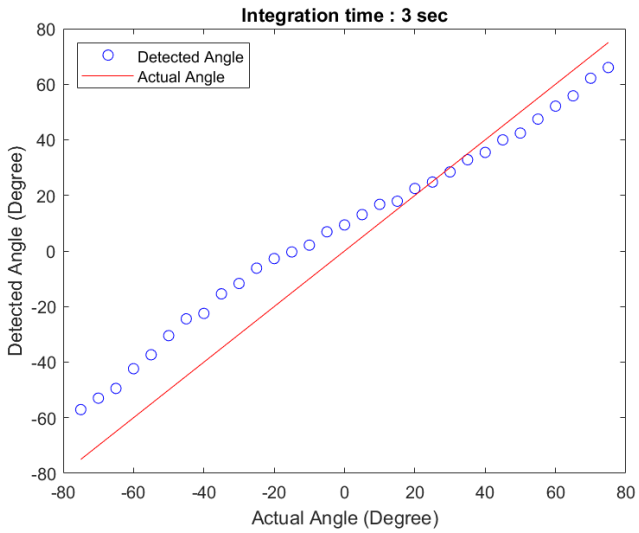

Figure 1. Comparison between detected and actual angle of arrival of a Yuneek Typhoon hovering nearby.

This result is significant since such detection has never been obtained before with colocated sensors having a total footprint of about 5 cm. This proof-of-concept, performed with the Yuneek Typhoon, represents only the first step in direction of arrival (DoA) determination of small multi-rotor UAVs by acoustic detection, without the need of sensor arrays or distributed sensors.

References

[1] C. Gabriel, C. John, and K. Matthew, "UAS detection, classification, and neutralization: Market survey 2015," Sandia National Laboratories, Livermore, CA, USA, 2015.

[2] R. Miles and Hoy, "Mechanically coupled ears for directional hearing in the parasitoid fly, Ormia ochracea ," *The Journal of the Acoustical Society of America*, *98*(6), 3059–3070, 1995.

[3] J. O. Mutton, "Acoustic ground sensors to triangulate bomb impact in support of airfield damage assessment," M.S. thesis, Dept. of Computer Science, NPS, Monterey, CA, USA, 2019. [Online]. Available: http://hdl.handle.net/10945/62813

[4] J. A. Feight, S. Whyte, J. D. Jacob, and R. J. Gaeta, “Acoustic characterization of a multi-rotor UAs as a first step towards noise reduction,” in *55th AIAA Aerospace Sciences Meeting*, 2017, p. 1174.

[5] T. Zhou, H. Jiang, Y. Sun, R. J. Fattah, X. Zhang, B. Huang, and L. Cheng, “Acoustic characteristics of a quad-copter under realistic flight conditions,” in *25th AIAA/CEAS Aeroacoustics Conference*, 2017, p. 2587.

ACKNOWLEDGMENTS

I am very proud to have successfully completed my thesis on detection of small UAVs using acoustic sensors, which is of interest to the Korean Navy and the U.S. military today. Through the process of study on theoretical learning, experimentation, analysis, and discussion, I was able to experience many things that I had never experienced in the last 10 years in the military, and I was able to expand my scope as an individual by considering things I had never thought about before.

And I felt that this positive result was something that I could never achieve alone. The project team that I joined was made up of really great people, Prof. Gamani Karunasiri, Prof. Fabio D. Alves, Dr. Renato Rabelo, Dr. Peter Crooker, and fellow project group members. Everyone was an expert on acoustic sensors, and the weekly meetings were very deep, serious, and advanced. The years of expertise that these top teams have accumulated have been a great help to me in conducting research. In particular, my advisor, Prof. Fabio Alves, gave me a clear direction for my research, and he taught me for hours and hours if I needed to learn research-related knowledge. I would like to thank again this wonderful team and Professor Fabio D. Alves.

Last, but not least, I would like to express my gratitude to my wife, Myungjin Hwang. She gave me a lot of support to complete my master's degree in the United States, a foreign country, and proceed with my thesis research. I want to express my gratitude and love for my wife.

THIS PAGE INTENTIONALLY LEFT BLANK

I. INTRODUCTION

A. BACKGROUND

Currently, small unmanned aerial vehicles (UAV) are being used in many areas, and in 2018, the number of small UAVs registered with the Federal Aviation Administration (FAA) alone exceeded one million. The total registration figure includes 878,000 hobbyists, who obtain a unique identification number for each small UAV they have, and 122,000 commercial, governmental, and other small UAVs, all of which are individually registered [1]. In particular, the market for commercial small UAVs is increasing more rapidly than anticipated, and could triple between now and 2023 [2].

With the advent of inexpensive commercially available UAVs, small UAVs are rapidly rising in popularity as is their growing variety of applications, ranging from shipping and delivery, the field of architecture for creating topographic surveys, photography, search and rescue, 3D mapping, and surveillance, to name only a few [1], [3].

While small UAVs have many uses, they also raise many problems because their use is unregulated. As a result, there is a great deal of interest in how to detect small UAVs in order to control their use. In fact, experiments and efforts to detect small UAVs are being implemented in many ways.

B. CURRENT PROBLEMS CAUSED BY SMALL UAVS

With the rise in small UAV availability, there has also been a growing number of incidents involving this type of aircraft, such as mid-air collisions, damage to property, and violations of privacy. In particular, small UAVs are increasingly flying in sensitive airspace, such as near airports, forest fire sites, and large congestion events, where their aircraft's existence alone can pose problems. For example, a small UAV crash-landed on the White House lawn [4] and another one, controlled by a German Pirate Party member, crashed in front of German Chancellor Angela Merkel [5]. This has added to the concerns about the safety of facilities and of political leaders.

Several cases of fire-fighting helicopters not being deployed to the scene of the fire because of private small UAVs flying in the area, resulting in much unpredicted damage, have been reported by [6], [7]. Small UAV crashes have also disrupted sporting events such as the U.S. Open tennis tournament as well as a World Cup skiing race [8], [9].

According to [10], "Between 19 and 21 December 2018, hundreds of flights were cancelled at Gatwick Airport near London, England, following reports of drone sightings close to the runway. With 140,000 passengers and 1,000 flights affected, it was the biggest disruption at Gatwick since its closure following the 2010 volcano eruptions in Iceland."

In the same way that small, multi-rotor UAVs can be explored as great assets in the defense realm, they pose a considerable threat to military operations as well [11]. “Enemy unmanned aircraft are among the biggest threats facing our ground troops today,” according to Dr. Thomas Bussing, vice president of Raytheon Advanced Missile Systems [11]. A clear example of this threat can be seen in North Korea’s activities against the South. Several small spy UAVs were found recently after they crashed [12], and North Korea is known to have hundreds of small UAVs capable of biochemical attacks [13]. Against this backdrop, many efforts have been conducted to prevent UAVs from performing surveillance, terrorist, or military attacks. Potential countermeasures cannot be employed, however, if the threat is not detected.

C. STATUS OF RESEARCH ON SMALL UAV DETECTION

A variety of approaches has been explored to interdict small UAVs; broadly classified, there are five types of effectors that could be used to deny a UAV mission. These include shooting missiles, guns, laser systems, electronic counter measures/high power microwave/high power electromagnetic weapons, and non-destructive techniques [14]. Nevertheless, in order for these countermeasures to be used, the UAV must first be detected and tracked.

Recent studies have sought to develop small UAV detection systems using radar, optics (i.e., cameras, infrared (IR)), acoustics, and radio frequency (RF) [14]. Each

approach has its own limitations. Although camera-based optics systems can cover long distances, they require good weather and bright conditions, high-performance lenses, and ultra-high-resolution cameras to detect small UAVs at a far distance. Furthermore, it is not easy to distinguish between small UAVs and birds, even after considering bird flight patterns, which small UAVs do not follow [15]. Thermal and IR imaging cameras for far distance are excessively costly and provide incomplete coverage because most current small UAVs are made of plastic and their electric motors do not emit much heat [14].

On the other hand, RF emission-based approaches may be useful for detecting most small commercial UAVs, which emit easily detectable signals, but they cannot address an RF-silent threat in autonomous navigation [14]. In addition, the use of Wi-Fi range (2.4–5 GHz) in no-license channels causes the presence of heavy interference [16]. Similarly, radar-based approaches can detect and track targets of a variety of sizes over kilometers of distance; however, the small UAV's radar cross-section is usually very small, so identification can be difficult with radar alone [14].

It is easy to observe that a common limitation of all of the aforementioned systems is the size of the target. One approach that is not affected by the size of the aircraft is acoustic detection. It depends on the sound emanated by the aircraft's rotors. Furthermore, acoustic detection is a completely passive system, which can be important in defense applications. Although many acoustic systems have been proposed for detection of small UAVs, as discussed in the next chapter, they commonly use conventional microphones, which suffer from detection-range limitations and require complex array arrangements for localization of the source [16].

Researchers from the Sensor Research Laboratory at the Naval Postgraduate School (NPS) have been investigating an approach to detect the presence and the direction of small UAVs using the microelectromechanical system (MEMS) directional acoustic sensors. In particular, *Ormia*-based MEMS sensors, used in a canted configuration, have proved to be very efficient in providing unambiguous directional detection of single-tone acoustic sources [17] and blast sounds such as bomb explosion and gunshots [18]. Benefiting from this knowhow, ***the objective of this thesis is to demonstrate the ability of colocated, canted, MEMS sensors to detect the bearing of a***

small UAV. These sensors have the advantage of possessing directionality proportional to the cosine of the angle of incidence, allowing the use of small sensor assemblies to obtain full angular coverage. These sensors exhibit very small form factor, low power consumption—even with the inclusion of amplification electronics—and high directional accuracy.

D. THESIS ORGANIZATION

As about 74 percent of all UAVs are multi-rotor [19], this study focuses on the acoustic detection and localization of small multi-rotor UAVs. A survey of the current methods, techniques, and technologies employed for acoustic detection of UAVs is provided in Chapter II. Advantages and drawbacks are highlighted, along with some figures of performance.

Next, in Chapter III, the acoustic signatures of small multi-rotor UAVs are briefly described. Specifically, the acoustic signature of a Yuneek Typhoon hexacopter is measured in an anechoic environment, and its specific spectral characteristics are identified.

Chapter IV provides a description of the *Ormia*-based MEMS sensor selected for the detection of the hexacopter in this study, including geometrical and acoustic characteristics as well as frequency, directional, and temporal response. Readout electronics are also briefly addressed.

Chapter V summarizes the employed technique and the experimental efforts to obtain an unambiguous detection on the direction of arrival. The impact of detection time is also studied. Concluding remarks are presented at the end of Chapter V, highlighting the accomplishments and discoveries of this research as well as areas recommendations for follow-on work.

E. BENEFITS OF THIS STUDY

Despite the many ways available to detect UAVs, no technology or methodology has shown outstanding capabilities in detecting small UAVs. Nevertheless, as small UAV detection research advances, some studies argue that acoustic detection will probably be

the most effective way [14]. In this realm, MEMS sensors, used at their resonances, might show some advantages compared to other acoustic sensors [17]. Compactness, low power consumption, mechanical noise rejection, high signal-to-noise ratio, as well as signature-based tunability are some characteristics of acoustic sensors to be explored in this study.

THIS PAGE INTENTIONALLY LEFT BLANK

II. CURRENT RESEARCH ON ACOUSTIC DETECTION OF SMALL UAVS

Recently, research on detection of small UAVs using acoustic means has gained attention and it has been conducted in various ways. Several research groups are interested in measuring, recording, and understanding the acoustic signatures of these aircrafts and eventually providing a library of such signatures for potential identification. A summary of some significant work found in the open literature is described in this chapter.

Feight et al. [20] reported on the acoustic signature of a typical quadrotor UAV (IRIS+). The measurements were done in an anechoic environment, using several microphones arranged in a circular pattern with the sound source in the center. They recorded different configurations such as rotor number and speeds. The authors concluded that narrow band spectra with strong spectral lines in frequencies below 5 kHz are dominated by the blade passing frequency (BPF) and its harmonics, which are the results of thickness load. The spectrum above 5 kHz is predominantly broadband due to a combination can coupling of various vibration sources. The contribution of an unloaded motor (i.e., one without blades) is minimal in the audible range when compared to the other sources. Finally, when hovering the aircraft showed an omnidirectional acoustic pattern, most likely due to its symmetric configuration.

While Feight et al. experimented in very controlled and static conditions, Zhou et al. [21] measured the acoustic characteristic of a quad-copter under realistic flight conditions, such as climbing, descending, cruising, and during yaw. They also used a rectangular microphone array inside an anechoic chamber, parallel to the ground, in addition to a second linear array that was placed vertically to provide insight about the sound emission along the propeller plane. The authors concluded that the overall characteristic of the spectrum is reasonably preserved for different regimes except for frequencies above 5 kHz where the forward flight spectrum showed some changes due to the complex coupling of all noise sources. To sustain forward movement, the propellers are driven at different speeds causing small shifts in the spectral lines of the BPF and its

harmonics, which is observed below 5 kHz. Most significant changes were found in the directivity pattern that showed higher sound pressure levels radiated towards the direction of travel.

Kloet et al. [22] expanded the analysis of small multi-rotor UAV acoustic characteristics such as detailed measurements of sound pressure levels (SPL), including their dependence on the distance and altitude, and corroborated that when the distance is doubled, a 6dB attenuation occurs. The authors also mapped the effect of orientation and determined that it is not significant when the sensors are away from the aircraft. For a hovering aircraft, the greatest SPL was found at 45 degrees of elevation. A thorough spectral analysis was conducted, including rotors with and without blades. Their findings are in agreement with [20] and [21].

Bernadini et al. [23] demonstrated that it is possible to detect the presence of small UAVs by signature identification, specifically using the correlation technique of audio fingerprinting. After measured signals were stored in digital form using acoustic sensors, short-term analysis of the sub-frames of 20 ms and mid-term analysis of the 200 ms window were conducted to perform decision making based on the machine learning technique. Using the recorded UAV sound and the environmental noise under different conditions, their research achieved UAV presence detection with 98.3% accuracy.

Similar work was performed by Fleming [24] who used a pre-trained convolutional neural network, AlexNet, to detect the presence of multi-rotor UAVs. Acoustic data under a large variety of conditions was collected and the continuous wavelet transform of the spectrograms were converted in image representations. The data, including several different aircraft in various flying regimes as well as background sound in a plethora of different environments, were used to train the AlexNet and evaluate its performance. Fleming concluded that the deep learning algorithm used could detect the presence of a small UAV flying at around 100 meters from the microphone with 94% accuracy.

Not many reports in the open literature address acoustic localization rather than signature measurement and analysis. In the following paragraphs, some interesting investigative work is summarized.

Pham and Sim [25] have demonstrated acoustic detection and tracking of small, low flying aircraft. They benefited from the strong harmonic structure also reported in [20] and [21] and used the incoherent wideband MUSIC (IWM) algorithm. Pham and Sim conducted their experiment using a 16-element cross array on the ground, with spacing of 1 ft. The strong harmonics between 100 and 200 Hz were used by the IWM to generate a main lobe coinciding with the bearing of the aircraft. Although their work provided the means to track the aircraft, the authors relied heavily on strong SPL provided due to diesel engines and a large array of microphones.

Jung and Ih [26] have demonstrated acoustic localization and tracking of multiple small multi-rotor UAVs. In their work, they used 3D acoustic intensity measurements from four MEMS microphones configured in a tetrahedral shape and calculated the cross power density between the corresponding signals. In addition, to compensate for spectral bias errors, which are fluctuations in the intensity spectrum due to the time-delay of the incident and reflected sound waves traveling between microphones, artificial intelligence algorithms were used. A three-frames-per-second nearly real-time bearing of a quadcopter was accurately measured in an anechoic environment. Benefiting from the differences in BPF of different multi-rotor aircraft, their bearings were determined almost simultaneously. The authors concluded that only when the BPFs are significantly different is discrimination possible.

Hommes et al. [27] have proposed the detection of a small UAV's direction of arrival (DoA) using acoustic antennas; however, this was not demonstrated, and the authors concentrated instead on studying the acoustic signature of the aircraft. In particular, doppler shifts on the BPFs due to the movement were mapped in addition to studies on Lloyd's mirror effect, which is the destructive interference due to reflection on the ground when the sensors are elevated. In their article, they proposed to study localization using an array of broadband MEMS microphones and non-colocated velocity estimations using finite differences of the measurements.

Zhang et al. [28] performed experimental studies of the acoustic characteristics of small multi-rotor UAVs over a runway using a phased array of 40 microphones with a total diameter of 6 m. Among their studies, identification and localization via beamforming techniques were proposed. The authors provided results for aircraft hovering near the array and a detailed analysis of the contributions to the spectral characteristics; they failed, however, to demonstrate reliable localization.

Blanchard et al. [29] characterized the acoustic signatures of small UAVs and estimated the 3D position using an orthogonal three-axis array with ten microphones. Particularly interesting, time-frequency delay-and-sum beaming (TFDSB) technology was applied to estimate the position of the aircraft under test. The experiment was conducted in an anechoic environment and outdoors as well. In the anechoic environment, due to the close proximity between target and sensors, about a ten-degree error in azimuth and elevation was found for most measurements when TFDSB was applied. During the outdoor measurements, the distance between the acoustic sensors and the aircraft was about 10 m and the elevation error was reduced to less than five degrees while the azimuth error significantly increased.

The common characteristic among all reported detection systems is the use of sensor arrays that do not have a small footprint. In addition, sophisticated algorithms and signal processing techniques are applied to provide rather limiting results. This shows that the acoustic localization of this type of target is not a simple problem. Benefiting from the knowhow detailed in the open source literature, we are conducting our own research and trying to demonstrate an unconventional method of small multi-rotor UAV acoustic localization without the need for arrays; rather we use two colocated sensors with a footprint no larger than a quarter dollar.

III. SMALL MULTI-ROTOR UAV ACOUSTIC SIGNATURE

A. BACKGROUND AND PREVIOUS WORK AT NPS

In the past few years, researchers form the Sensor Research Laboratory have been recording the general acoustic of various Class I/II small UAVs, both in a laboratory setting and in the field. Various flight regimes and loads were used to capture the broadest possible data set. Each of the tested aircraft cost less than $800 and was selected for both ease of operation and commercial availability. A few examples of the studied UAVs are the DJI Inspire Pro, DJI Phantom 3, DJI Phantom 4, DJI Mavic, and the Yuneec Typhoon, some of which are shown in Figure 1. These small UAVs are four or six rotating wing-type aircraft weighing 1 to 2 Kg, and possessing similar design characteristics of more than 90 percent of the quad/hexa-copters on the market.

The flight regimes of a multi-rotor, vertical take-off and landing (VTOL) aircraft can be divided into three types [20]. Axial flight is the pure vertical climbing or descending action, where the axes of the rotation of the rotors are aligned with the direction of the airflow. Non-axial flight occurs when there is a horizontal component to the aircraft movement, or the air flow is not aligned with the axes of the rotors. Finally, hover occurs when the aircraft is maintaining the same position and altitude.

In the laboratory, the data collection was performed at Naval Postgraduate School's anechoic chamber[1] (Figure 2b), which is capable of absorbing 99 percent of incident acoustic waves above 100 Hz [30]. This study was only performed in hovering regime due to limitations in the size of the anechoic chamber. Different loads for each UAV were used. In the field (Figure 2a) acoustic signature data collection was performed in isolated fields far away from most urban background noise. All three flight regimes with different loads were studied in the field and an extensive library of acoustic signatures was collected.

[1] Absorption characteristics of the NPS anechoic chamber were measured in October 2017 by engineers of PCB Piezotronics.

Figure 1. Examples of studied UAVs, from left to right: DJI Phantom; DJI Mavic; DJI Yuneec Typhoon.

Although the detailed results are not available for public distribution, the general result of the data analysis shows that common acoustic spectral characteristics of most of the flight regimes and different loads were found within a specific range of frequencies. Therefore, in order to conduct this study, one particular small UAV was selected (the Yuneek Typhoon) without loss of generality.

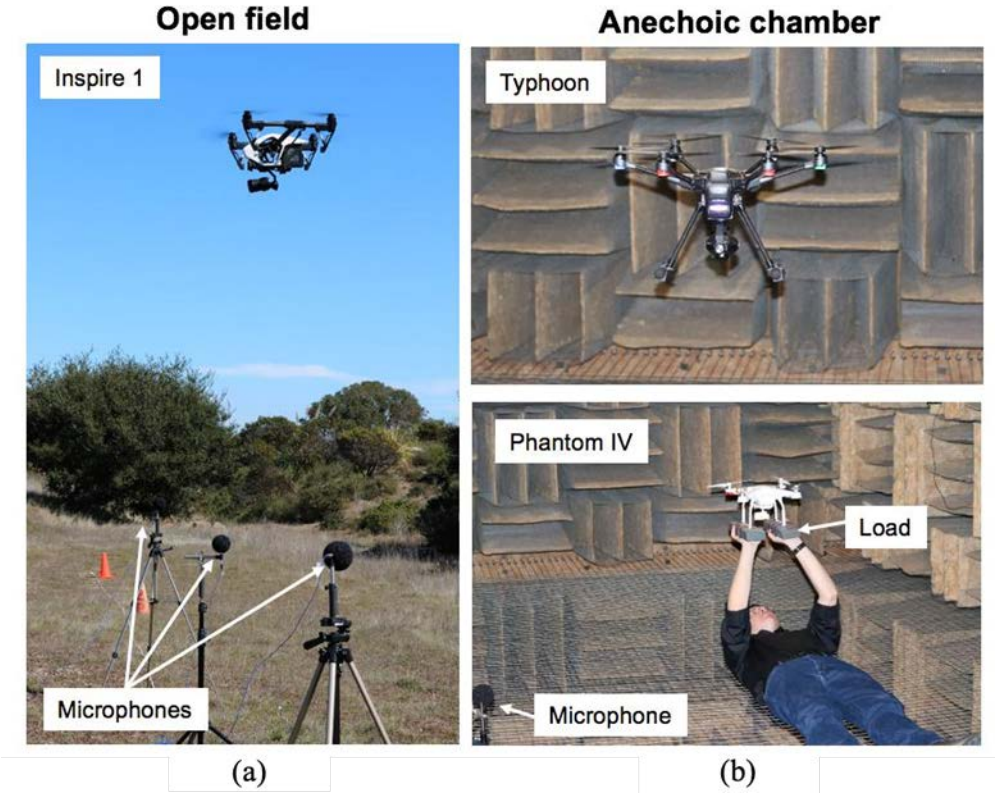

Several multi-rotor small UAVs were tested in various flight regimes.

Figure 2. Environments used to collect the acoustic signature of small UAVs.

Acoustic noise from the UAV rotors is typically divided into three categories: thickness noise; quadrupole noise; and loading noise [31]. Thickness noise is caused by the displacement of air as the blade spins and depends on the shape and aerodynamic profile of the blades. This noise propagates on the plane of the rotor, and it is not apparent below and above it [31]. Quadrupole noise arises from trailing edge wake flows, boundary layer flows, and other flow mechanisms, and it is normally weaker than the other noise sources, except at lower rotor tip velocities. This noise is broadband in nature. Finally, the loading noise is due to the lift and drag (forces exerted in the air by the airfoil). This noise predominates above and below the rotor and does not propagate in the plane of the rotor. In non-axial flight regimes, loading noise tends to be unsteady due to the fuselage interaction and the vortex caused by the other rotors.

Although there are vast possibilities to study the details and intricacies of the multi-rotor aircrafts' acoustic signatures, this thesis concentrates on the general characteristics of the sound generated by a particular small hexacopter (Yuneek Typhoon) in hovering regime inside an anechoic chamber. Detailed analysis of spectral features is left for future work.

B. ACOUSTIC SIGNATURE OF THE YUNEEK TYPHOON

A temporal response (time series), average spectrum, spectrogram, and 3D spectrogram of the Yuneek Typhoon, shown in Figure 3, were obtained from measurements in the anechoic chamber while the aircraft was made to hover about two meters form a calibrated microphone. The detailed information on the instrumentation and experimental setup is given in Chapter V. The measurements were taken in 30-second windows, and one of the runs is shown for a frequency range between 300 and 5000 Hz. Spectral lines around specific frequencies are clearly identifiable as is the temporal variation around the average frequencies. The spectral lines are well separated between 300 Hz and 2 kHz and start to fade between 2 and 3 kHz. After 3 kHz, the lines are no longer well separated, and frequency discrimination becomes difficult.

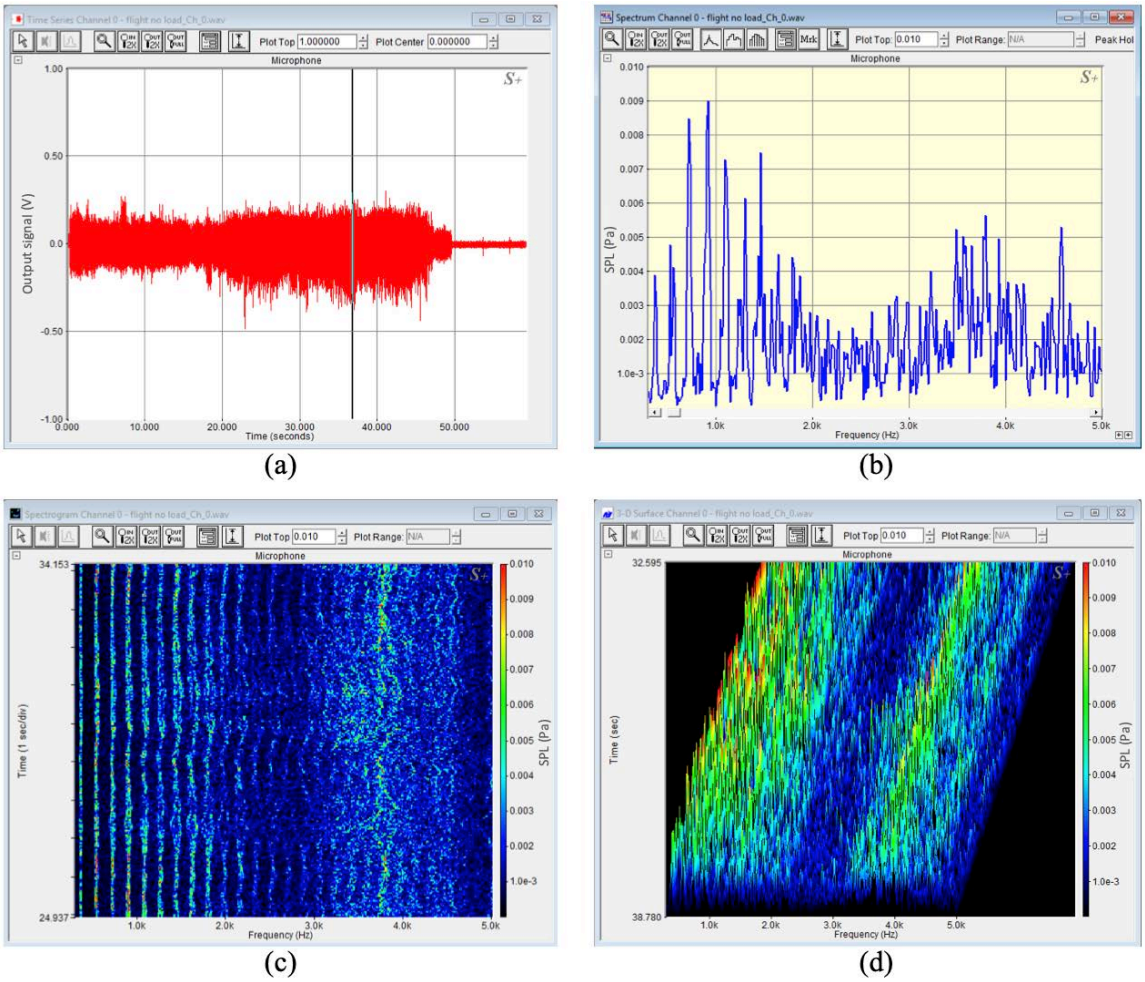

(a) Time series; (b) spectrum; (c) spectrogram; and (d) 3D surface spectrogram of a Yuneek Typhoon, measured in an anechoic chamber, in the frequency range between 300 and 5000 Hz

Figure 3. Acoustic signature of the Yuneek Typhoon.

Figure 4 presents the spectrum and spectrogram details in a much narrower band (300 to 1300 Hz) where the stronger harmonics were found. Notice that a strong signal was found to be around 700 Hz.

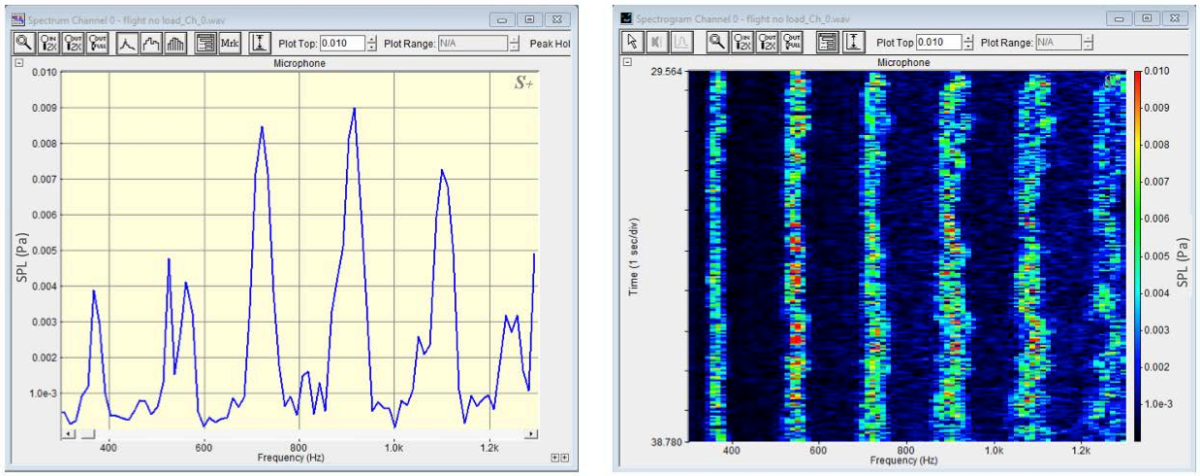

(a) Spectrum and (b) Spectrogram of a Yuneek Typhoon measured in an anechoic chamber, in the frequency range between 300 and 1300 Hz

Figure 4. Spectrum and spectrogram of a Yuneek Typhoon in narrower band.

The jitter around a specific frequency and its harmonics can identify small variations in rotors' rotation speed as changes are made to keep the desired flight regime.

The sound pressure level was found to be around 5 mPa on average for the stronger spectral line (100 Hz bandwidth) and did not change much as the aircraft was loaded (not shown). The average frequency slightly increased due to the faster rotation necessary to compensate for the weight of the aircraft.

Based on these characteristics, an *Ormia*-based MEMS acoustic directional sensor was designed to exhibit resonant response around 700 Hz, to match the strong emission of the source. One advantage of operating at resonance while having a frequency response matched with the bandwidth of the spectral line of the source intended to be detected is the ability to naturally filter out a large portion of undesirable background noise.

Specifications of the sensor and its readout electronics, as well as a detailed characterization of its acoustic properties, are provided in the next chapter.

IV. *ORMIA*-BASED MEMS DIRECTIONAL SENSOR

Researchers from the sensor research laboratory at NPS have been designing and demonstrating the use of *Ormia*-based MEMS directional sensors for different applications [17], [32–33]. A detailed explanation on how the sensors work and mathematical models can be found in [17], [33]. Essentially, the MEMS sensors, which mimic the hearing system of the *Ormia Ochracea* fly, exhibit two dominant oscillatory modes, rocking (seesaw movement), where both wings move out of phase, and bending (flapping movement), where the wings move in phase. Both oscillation modes depend on the direction of arrival (DoA) of the acoustic source. While the bending mode depends on the cosine of the angle of incidence, the rocking is in quadrature. Using a single mode gives an ambiguous DoA since the cosine is symmetric at about zero and the sine is symmetric at about 90 degrees. The fly utilizes both modes and with a single hearing system obtains the DoA of specific tones.

In previous work[2] [30], MEMS sensors have been designed with spectral response characteristics to match the stronger spectral lines from the Typhoon signature. The sensor micrograph taken in a scanning electron microscope (SEM) with the details for interdigitated capacitive comb fingers on the edges is shown in Figure 5. In the figure, the numbers indicate the following parts: (1) wings; (2) bridge (connects both wings); (3) torsional leg (connects the entire structure to the substrate); (4) substrate (where the structure is anchored); and (5) interdigitated capacitive comb fingers (provide differential capacitance for electronic readout). For this task, bending motion was selected due to its intrinsically larger oscillation amplitudes (higher sensitivity).

This sensor was designed using a multiphysics finite element application (COMSOL) and fabricated using a commercial foundry, MEMSCAP, through their SOIMumps process [34].

[2] Karunasiri, G. and Alves, F., "MEMS directional acoustic sensor for small UAV localization," 2019, unpublished.

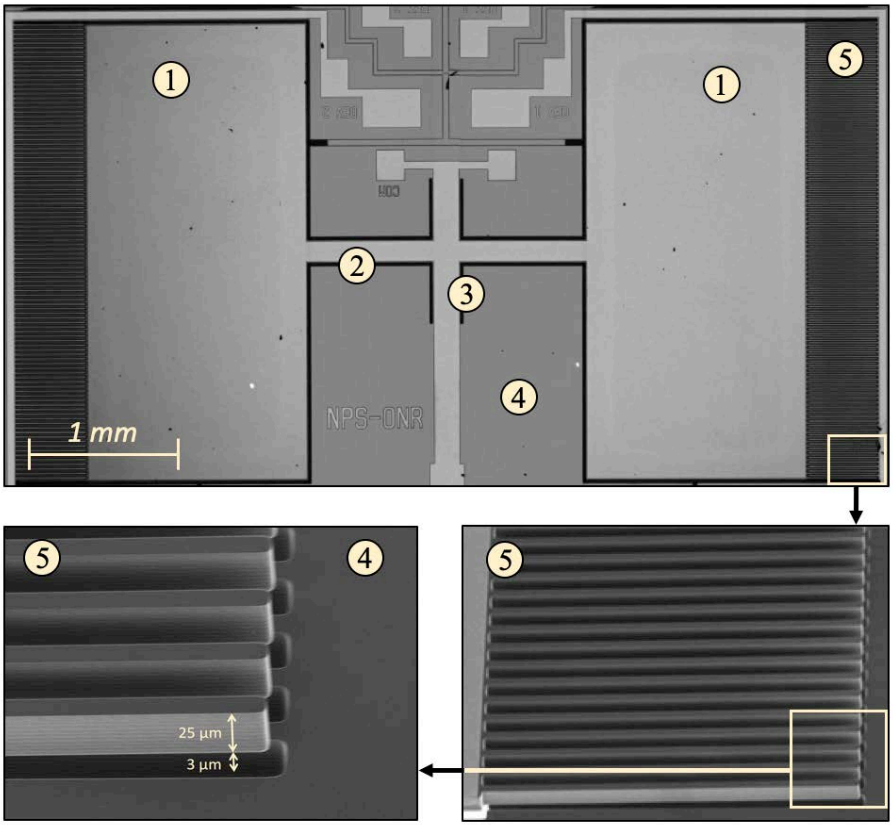

See legend explanation in the text.

Figure 5. SEM micrograph of the *Ormia*-based MEMS acoustic sensor.

The spectral response of the sensors can be controlled by design by tailoring geometrical characteristics, such as overall size, bridge and leg length and width, as well as device thickness.

Interdigitated capacitive comb fingers are placed on the edge of each wing as well as on the neighboring substrate. When the wings oscillate in response to acoustic stimulus, the capacitance changes proportionally since the substrate remains static. An electronic circuit reads out the change in capacitance and converts it into voltage.

Although several sensors were fabricated with the same dimensions in the same wafer, non-uniformities in the processes can cause slightly different responses even in adjacent devices. Once received from the foundry, the sensors were integrated with the readout electronics. Figure 6a shows the sensor cemented on a printed circuit board

(PCB), wirebonded to the amplification electronics. A simplified diagram of the charge-to-voltage conversion is shown in Figure 6b.

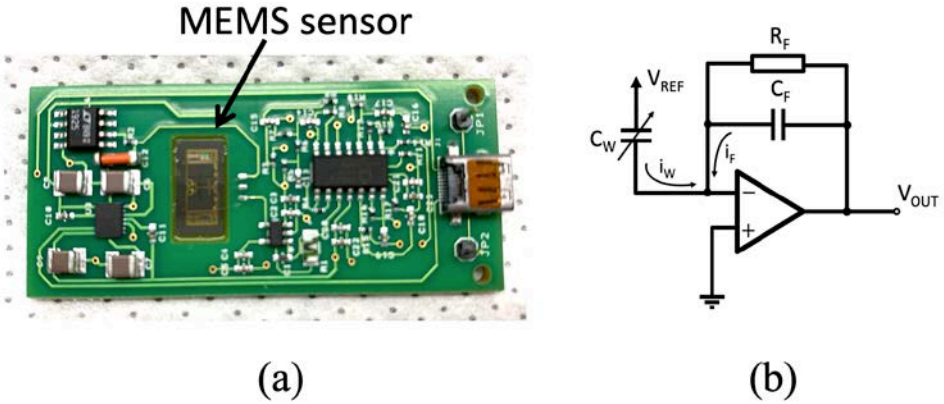

(a) MEMS sensor mounted on the electronic readout PCB, and (b) simplified schematic diagram of the charge amplifier used to covert capacitance in voltage.

Figure 6. MEMS sensor and printed circuit board (PCB).

The voltage output (V_{OUT}) varies with the change in capacitance from the comb fingers according to

$$\Delta V_{OUT} = \frac{V_{REF}\Delta C_W}{C_F} \quad (1)$$

where V_{REF} is a reference voltage used to bias the sensor comb finger capacitors, C_W is the capacitance of the sensor wings, and C_F is the feedback capacitor. In the circuit, R_F is a compensation resistor with a large resistance that can be considered an open circuit. The advantage of this approach is that at rest, V_{OUT} is zero and it remains zero as long as there is no acoustic stimulus, despite temperature and illumination variations on the sensor board.

To accomplish the objective of this research, a pair of sensors with matching properties must be found; therefore, once received from the foundry, several sensors were characterized following the procedures described in the next section.

A. CHARACTERIZATION OF THE SENSORS

The characterization process is fourfold. Frequency response, sensitivity, directionality, and noise were measured while the sensor was mounted on a turntable inside the NPS anechoic chamber. Figure 7 shows a schematic diagram of the experimental setup.

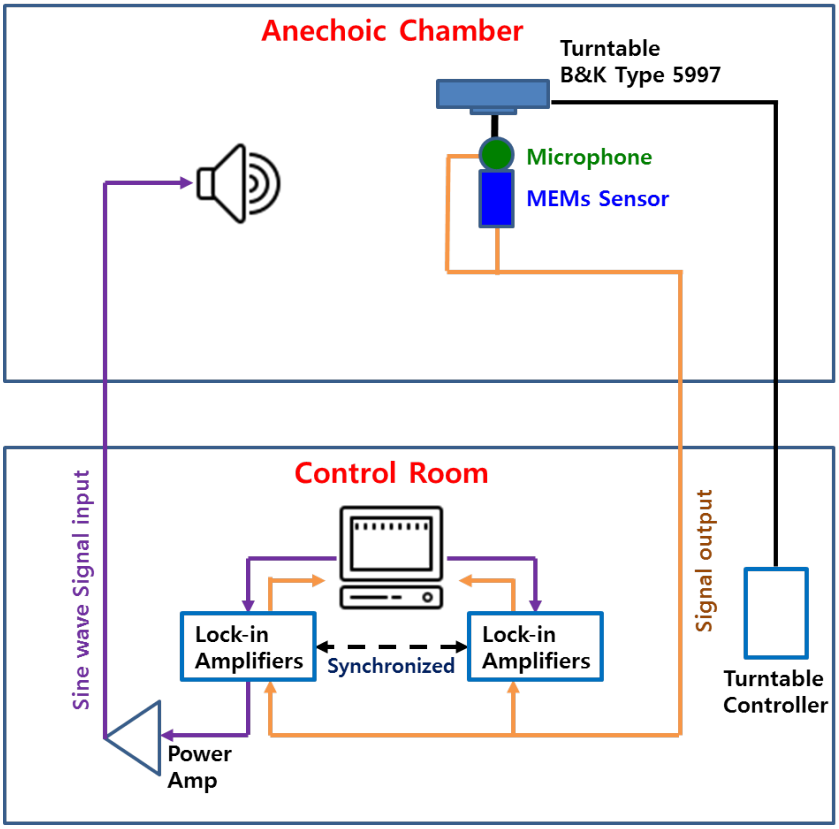

Figure 7. Schematic diagram of experimental setup used for sensor characterization.

The sensor readout electronics are powered by a standard power supply (9 V) and their output was connected to a lock-in amplifier (Zurich Instruments MLFI 500 kHz), controlled by a LabOne Web Server application, launched in the host computer where the data was recorded. The lock-in amplifier provides an output frequency (internal reference) that excites a speaker (JBL 2380A Bi-radial horn) through the audio amplifier. The turntable has an electronic controller (B&K Type 5997) that allows for precise

angular placement or continuous rotation of the senor under test. A calibrated microphone (PCB 378A21), preconditioned by a PCB Piezotronics signal conditioner model 482C set to provide gain 100, was colocated with the MEMS sensors to provide the sound pressure level. The microphone was connected to a second lock-in amplifier. Both lock-in amplifiers were synchronized and the setup could then be used to perform all necessary measurements.

B. FREQUENCY RESPONSE

Initially, frequency response was measured individually, by sweeping the speaker stimulus from 100 to 1500 Hz. The sensors were placed individually in the turntable mandrel with a 3D-printed mount attached to a metallic half-inch rod as shown in Figure 8a.

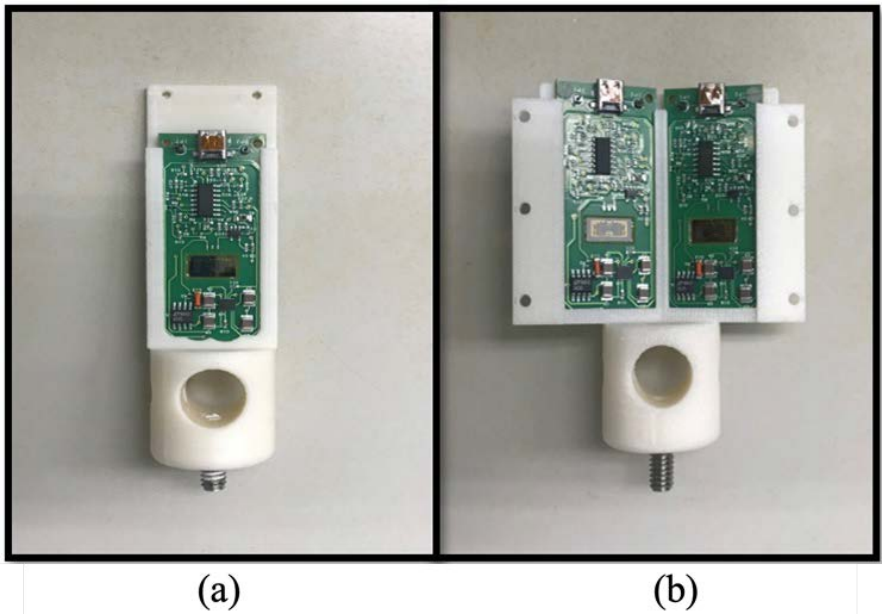

Figure 8. Sensor placement: (a) single mount and (b) canted mount.

The sensors were arranged to assure normal incidence (DoA=0 degrees) and stimulated at resonance until saturation was achieved. The speaker amplifier was set to provide a sound level slightly below saturation and the frequency sweeps were performed. Figure 9 shows the frequency response of the sensor 6–1-1, named for its fabrication

generation, design sequence, and position in the wafer. In Figure 9, the left side shows the output voltage of the readout circuit (V_{OUT}) and the right side shows the sensitivity in volts per pascal, obtained by dividing the output voltage by the sound pressure level, measured by the co-located calibrated microphone.

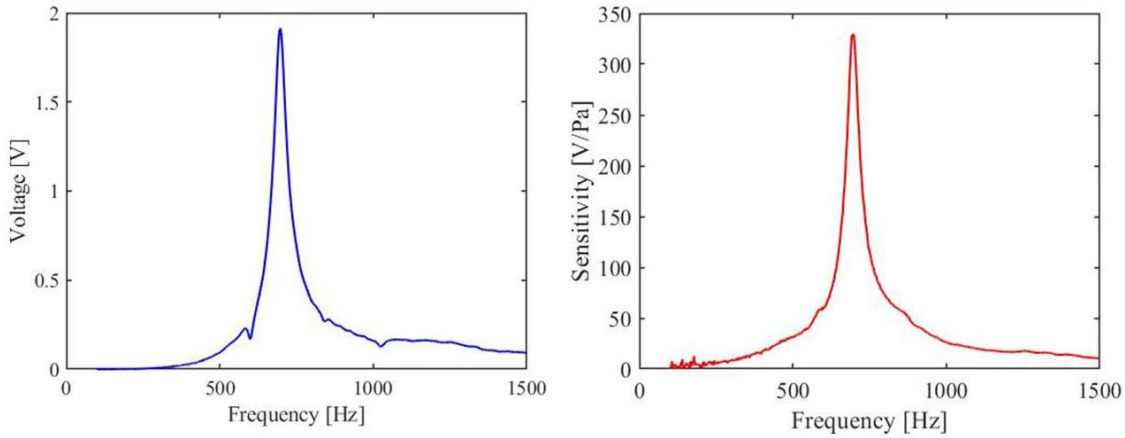

The overall response is derived from the bending mode.

Figure 9. Frequency response of the of the 6–1-1 sensor: voltage output (left) and sensitivity (right).

From Figure 9, the resonant behavior of the sensor is clear in bending mode. There is no rocking motion when the sensor is excited in normal incidence. In addition, even away from normal incidence, the rocking mode is very small (~10 times less) as compared with the bending mode [17].

Subsequently, the sound pressure level of the acoustic stimulus was reduced to one-half of the initial value and to zero to verify the linear behavior of the sensor as well as the noise floor. Figure 10 shows the sensitivity of sensor 6–1-1 under these conditions, in logarithmic scale to show the noise floor.

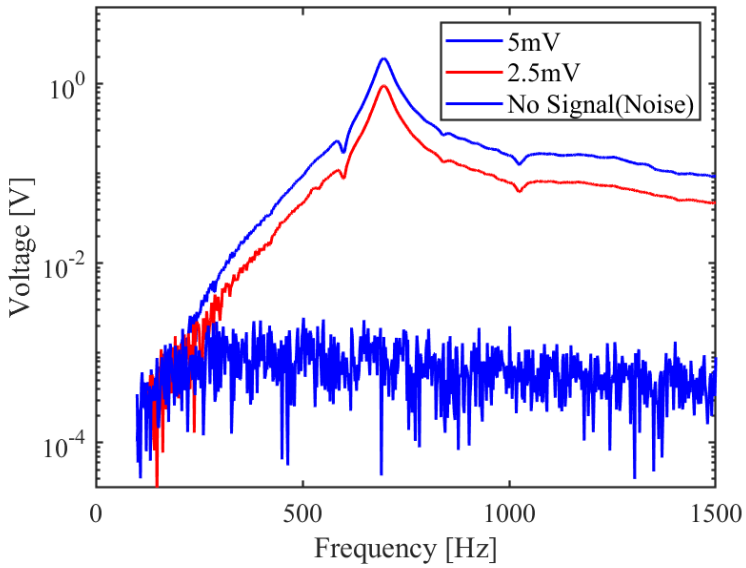

Notice that the sensitivity is given in logarithmic scale.

Figure 10. Frequency response of 6–1-1 sensor by input signal amplitude.

Several sensors were tested and the best match in frequency response was found between sensors 6–1-1 and 6–1-4. Maximum sensitivity of 329 V/Pa was found to be at 696 Hz for sensor 6–1-1 and 344 V/Pa at 691 Hz for sensor 6–1-4. The full width at half maxima (FWHM) was about 100 Hz for both sensors.

Figure 11 shows the comparison in frequency response between sensors 6–1-1 and 6–1-4. It can be seen that they have almost identical responses to frequencies from 100 to 1500 Hz, with only a 5 Hz shift. A small difference in amplitude is also noticeable, and it is most likely due to misalignment when positioning the sensors for normal incidence measurements.

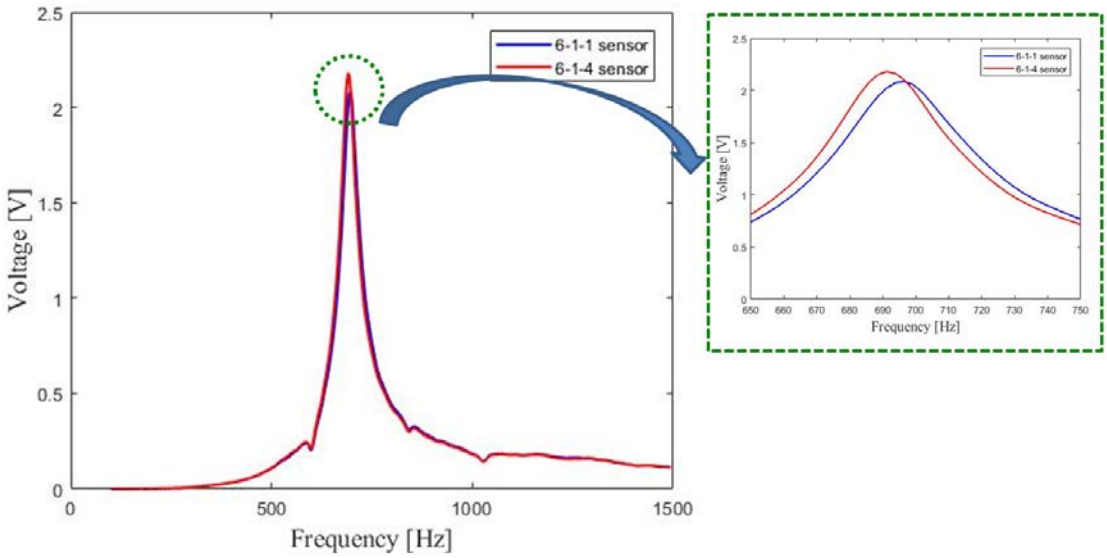

The small visible difference in amplitude (dashed circle) is most likely due to misalignment when positioning the sensors for normal incidence measurements.

Figure 11. Comparison of frequency response between the 6–1-1 and 6–1-4 sensors.

C. DIRECTIONAL RESPONSE

The same experimental setup was used to obtain the directional response of the sensors at the bending frequency (maximum sensitivity). The calibrated microphone was removed since the sensitivity of each MEMS sensor is already known. The sensor is fixed to a single mount and placed in an orthogonal position with the speaker, and this orthogonal state was set to the initial orientation value of 0 degrees and rotated from -130 degrees to 130 degrees at a rate of 360 steps per rotation.

Figure 12 shows the measured directional response of the sensor 6–1-1 for two levels of acoustic stimulus (near saturation and one-half of that), both showing a cosine dependence of the angle of arrival. As expected, the maximum output was achieved at zero degrees, and the minimum voltage was achieved at -90 degrees and 90 degrees. It is observable that the directional responses are not completely smooth. This is due to the turntable rotation that causes a vibrational mode that couples with the sensor near resonance. We have noticed that this noise is not present when measuring sensors that resonate at higher frequencies (> 1 kHz).

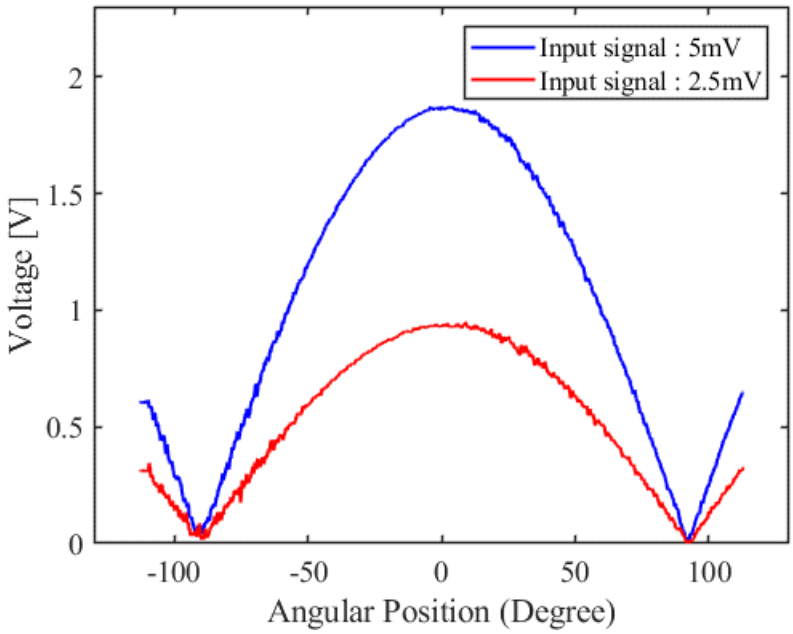

Figure 12. Directional response of 6–1-1 sensor at two different stimulation levels.

Figure 13 shows the directional response of both sensors, 6–1-1 and 6–1-4, simultaneously measured while the sensors were mounted in a canted angle of 15 degrees (see Figure 8b). The graphs clearly show the shift in angle of 30 degrees between sensors as well as a very symmetric response. This result is what was desired for the unambiguous DoA determination, which is detailed in the next chapter.

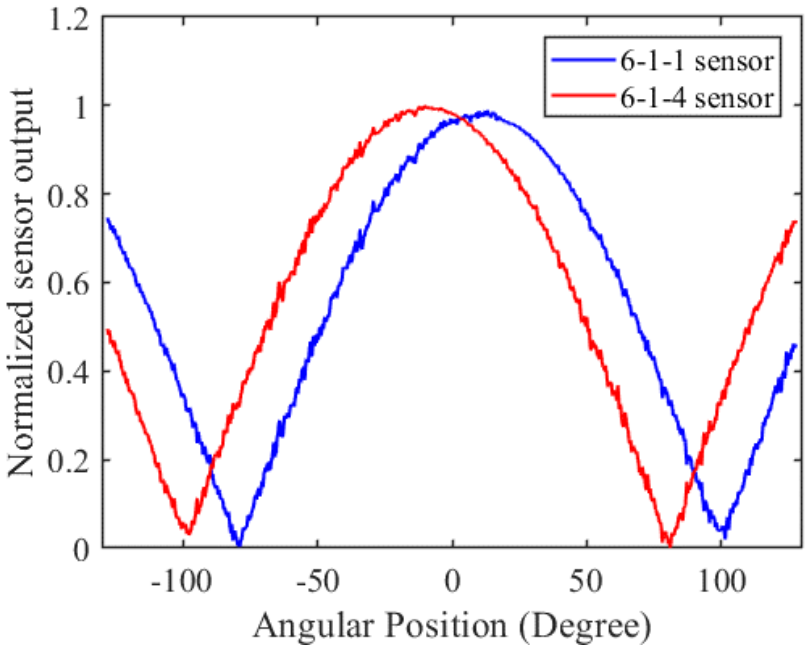

Arranged in canted angles with 15 degrees offset (see Figure 8b).

Figure 13. Simultaneous directional response of sensors 6–1-1 and 6–1-4.

THIS PAGE INTENTIONALLY LEFT BLANK

V. UNAMBIGUOUS DETERMINATION OF THE DIRECTION OF ARRIVAL

A. DIRECTIONAL RESPONSE OF CANTED ANGLE SENSORS

In the fly's head, there is a closed cavity with special features to control the influence of both the rocking and bending oscillatory modes. In our open-back configuration, there is no such cavity and the bending mode is dominant. Furthermore, because the acoustic waves interact with both sides, front and back, the MEMS sensor, at the bending frequency, performs as a pressure gradient microphone with predicted cosine dependence of the amplitude of vibration on the sound direction [35]. If the incident sound pressure amplitude at the sensor is P_0, then the output voltage (V_{OUT}) as a function of incident angle has the form of

$$V_{OUT} \propto |P_0 \cos(\theta)| \tag{2}$$

Figure 14 shows Equation (2) compared with the experimental directional response of sensor 6–1-1. Both curves are normalized. A perfect agreement can be observed, corroborating that the model precisely describes the sensor response for a single-tone excitation.

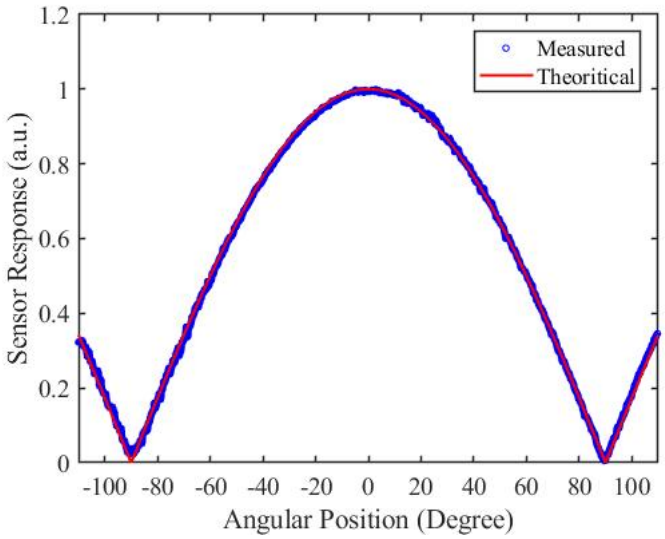

Figure 14. Theoretical and measured directional response of MEMS sensors.

A clear conclusion from Figure 14 is that ambiguity at zero degrees is due to the parity of the cosine function. In this case, it is impossible to determine whether the acoustic source is at the right or left side. Furthermore, if the sound intensity of the source is changing (P_0 not constant), there is no way to determine direction.

A simple way to solve both problems is to employ two sensors configured in a canted angle, as has been suggested in previous sections.

Figure 15 shows a schematic diagram of two canted sensors where the DoA for the sensor on the left is the angle of arrival plus the offset angle with respect to the normal, and the DoA for the senor on the right is the angle of arrival minus the offset angle.

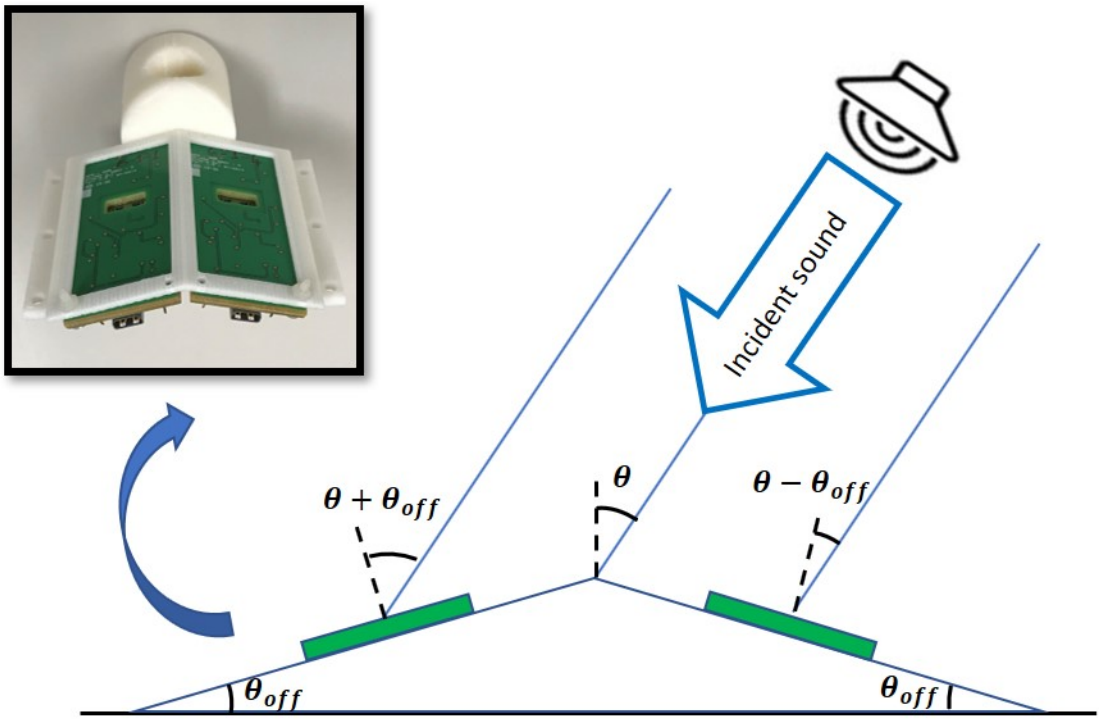

Figure 15. Arrangement of two canted MEMS DF sensors.

Since the P_0 is virtually the same at both sensors (the distance between two sensors is much smaller than the distance from the source), each sensor has an output value compensated by the offset angle (θ_{off}), mathematically represented by

$$V_L \propto P_0 \cos(\theta - \theta_{off}) \text{ and } V_R \propto P_0 \cos(\theta + \theta_{off}),$$
$$for -90° + \theta_{off} \leq \theta \leq 90° - \theta_{off} \quad (3)$$

Here, the index L represents the left side and the index R represents the right side.

Based on Equation (3), the cosine-type output of each sensor will show a shift equal to twice the off-set angle of the sensors. Figure 16 shows a plot of Equation (3) for an offset angle of 15 degrees. A shift in angle of 30 degrees is easily observed.

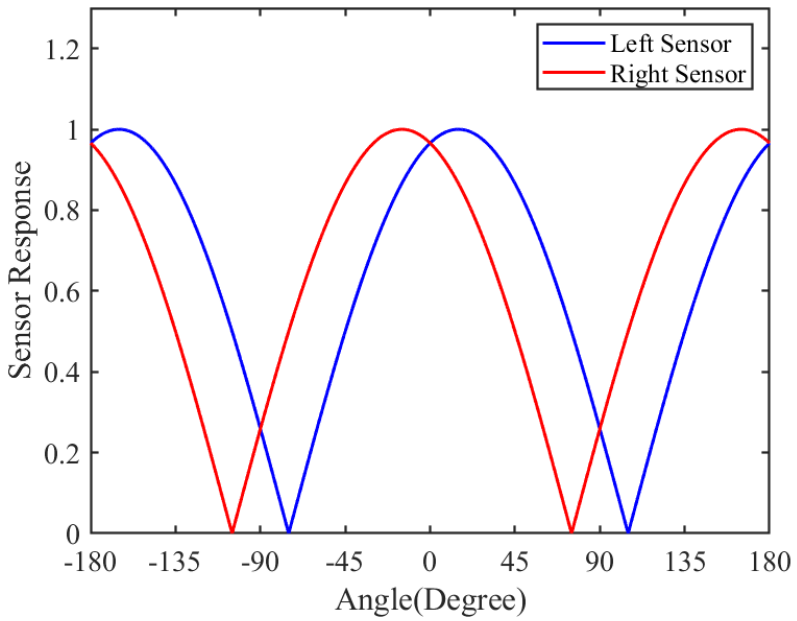

Figure 16. Theoretical response canted sensors at 15 degrees offset angle.

Taking the difference over the sum of the outputs of both sensors we obtain

$$\frac{V_L - V_R}{V_L + V_R} = \left(\frac{\cos(\theta - \theta_{off}) - \cos(\theta + \theta_{off})}{\cos(\theta - \theta_{off}) + \cos(\theta + \theta_{off})}\right),$$
$$for \ -90° + \theta_{off} \leq \theta \leq 90° - \theta_{off} \quad (4)$$

Equation (4) can be simplified using well-known trigonometric identities to

$$\frac{V_L - V_R}{V_L + V_R} = \tan(\theta_{off})\tan(\theta) \tag{5}$$

Solving Equation (5) for θ, we obtain

$$\theta = tan^{-1}\left(\frac{1}{\tan(\theta_{off})} \times \frac{V_L - V_R}{V_L + V_R}\right)$$
$$for\ -90° + \theta_{off} \leq \theta \leq 90° - \theta_{off} \tag{6}$$

Since arctan is antisymmetric about zero, the ambiguity in determining the DoA has disappeared, as shown in Figure 17. Furthermore, it is no longer necessary to know the sound pressure level at the sensor location.

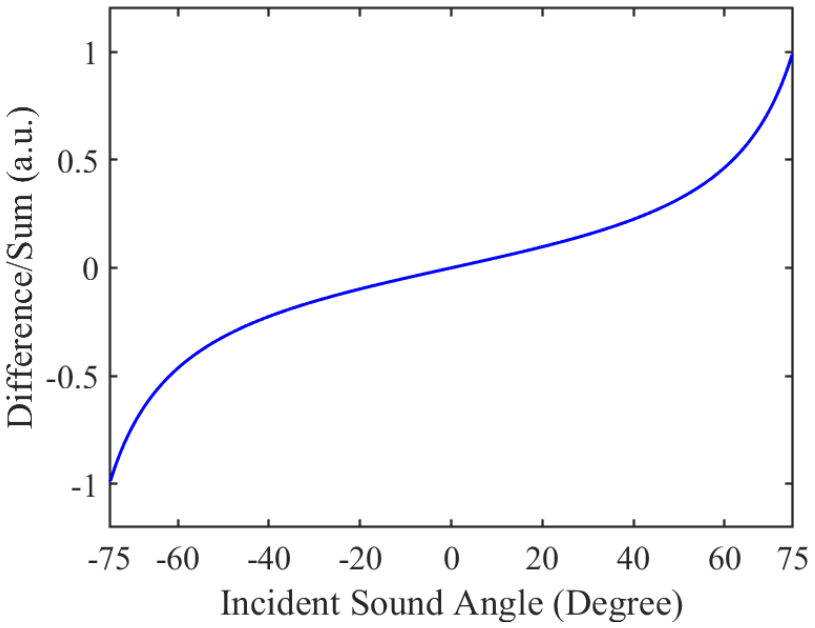

Figure 17. Difference over sum output for canted sensors at 15 degrees offset angle.

This is a simple, albeit elegant, way to provide unambiguous DoA of acoustic tones using *Ormia*-based sensors operating in bending mode. It works well for single-tone signals and synchronous demodulation (lock-in) being applied so far.

B. DOA DETECTION OF THE YUNEEK TYPHOON UAV

For UAV detection, initially we tried synchronous demodulation, using the experimental setup already in place. In order to simplify the measurement efforts and assure that the MEMS sensor would not be compromised by dust due to the aircraft propellers, recorded sound was used instead. This was instrumental to allow long runs without battery replacements and damaged sensors. A 30-second wave file with the Yuneek Typhoon's sound recorded in the anechoic chamber was played using the same speaker and acoustic amplifier described in Chapter IV, Section A.

Initially, only sensor 6–1-1 was used, and its directional response to the UAV sound is shown in Figure 18. The file was played in repeated mode so it would not stop during the rotation, which was performed from -130 degrees to 130 degrees at a rate of 360 steps per rotation.

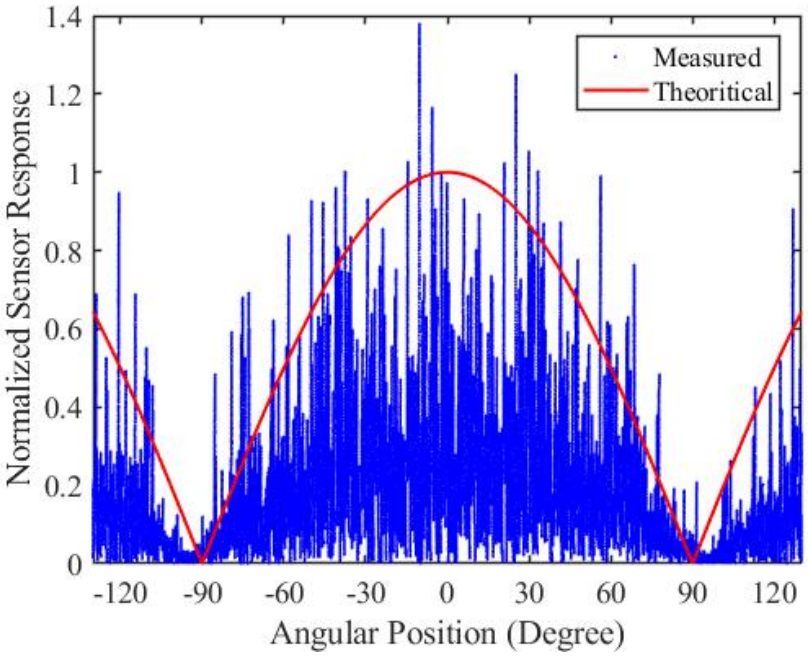

Sensor response was recorded by a lock-in amplifier and normalized.

Figure 18. Theoretical and measured response of MEMS sensor to the small UAV sound.

The theoretical response is overlapped with the measured data to show the trend. Clearly the minima can be identified as well as the cosine trend of a very noisy response. This is easily explained by the characteristics of the measurement. In synchronous demodulation, only the reference frequency (set to the maximum response of the MEMS sensor) is captured by the lock-in. Since there is a strong jitter around the center frequency, the through signal is eventually captured, but it often goes back to zero or a random value in between the theoretical and zero. This result makes it very difficult to predict direction even with knowledge of the sound pressure level at the sensor location.

As can be observed in Figure 4, the jitter span around 700 Hz is about 100 kHz, which matches the FWHM of the MEMS sensors (Figure 9). Therefore, if the signal can be captured over the entire band of sensitivity of the sensor and integrated for averaging purposes for a few seconds, the directional characteristic would be enhanced. Furthermore, since the detection scheme uses two sensors detecting the sound simultaneously, the temporal variations in intensity of the incoming signal would be perceived equally by both sensors. When applied to Equation (6) it would provide, in theory, an accurate DoA value.

In lieu of synchronous demodulation, a data acquisition system (DAS), Spectrum Devices DT9837A (14-bit analog to digital converter), controlled by the SpectraPLUS-DT FFT spectral analysis suite installed on a host computer, was used (see Figure 19).

Initially, the Typhoon recording was played for a few seconds and measured using sensor 6–1-1. Figure 20 shows the spectrum and the spectrogram of the detected signal from 300 to 5000 Hz. It is clear from the figure that most of the signal outside of the 700 Hz resonance was naturally filtered out. This constitutes a great advantage since outside of the anechoic chamber background/environmental noise will be present and it will be significantly reduced by the narrow band detection. Compare Figure 20 with Figure 4.

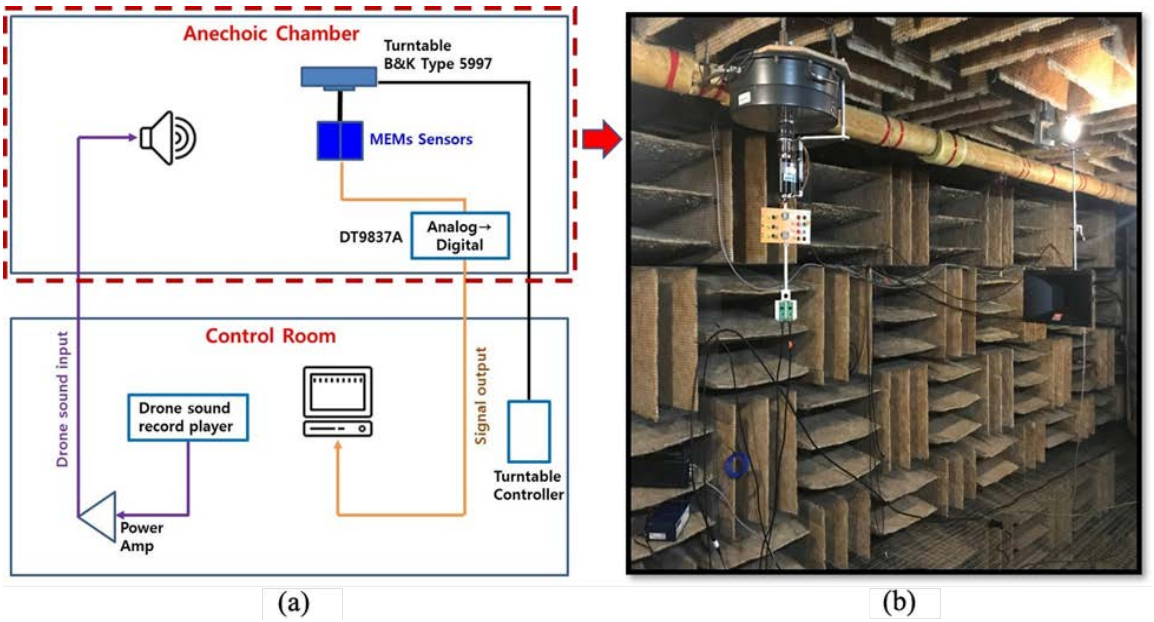

(a) Schematic diagram and (b) photograph of anechoic chamber test for directional measurement of small UAV direction of arrival using a DAS.

Figure 19. Schematic diagram of experimental setup used for directional test.

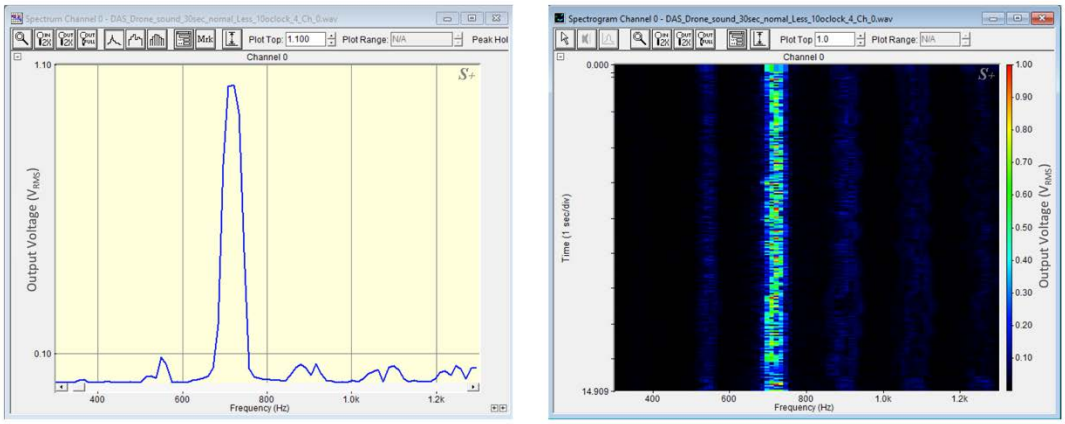

Measured in an anechoic chamber, in the frequency range of 300 to 5000 Hz, by the MEMS sensor 6–1-1

Figure 20. Detected signal from a Yuneek Typhoon:
(a) spectrum, and (b) spectrogram.

Next, the same sensor, under the same excitation, was rotated from -120 to +120 degrees in relation to the normal and the signal was measured in the same way. Figure 21 shows the time series and the spectrogram of the measured signal.

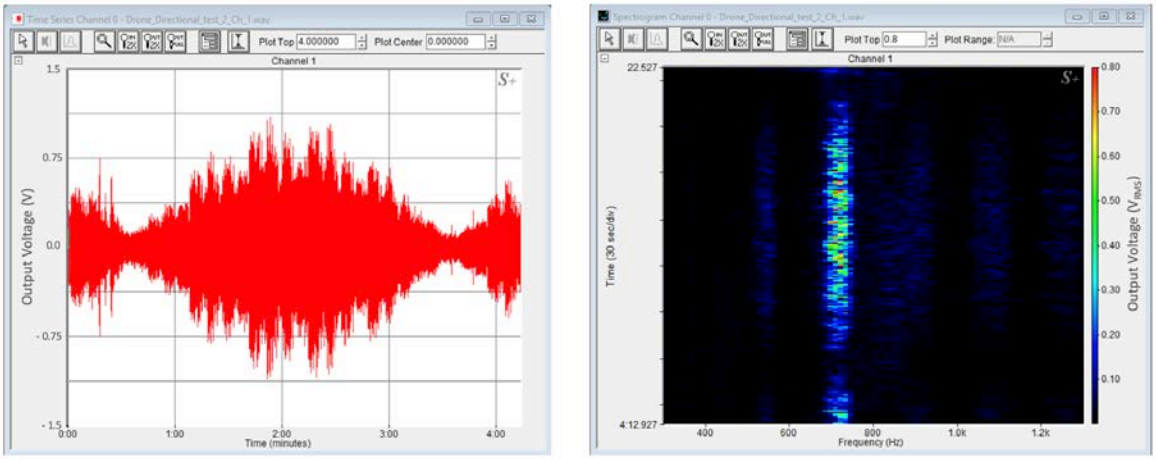

(a) (b)

Measured in an anechoic chamber, by the MEMS sensor 6–1-1, rotating from -120 to 120 degrees

Figure 21. Measured signal from a Yuneek Typhoon: (a) time series and (b) spectrogram.

It is easy to observe the directional dependence of the sensor in the time series and the spectrogram, where the two minima correspond to -90 and +90 degrees and the region of maximum surrounds normal incidence. This shows that detection is frequency selective and directional dependent, as expected. The minima are not zero due to coupling vibrations in the sensor mount, vibrations due to the rotating turntable (as seen before), and alignment imperfections.

The same procedure was repeated with both sensors simultaneously. The output voltages of sensors 6–1-1 and 6–1-4 at normal incidence are shown in Figure 22a and 22b, respectively. Clearly, the responses are almost identical.

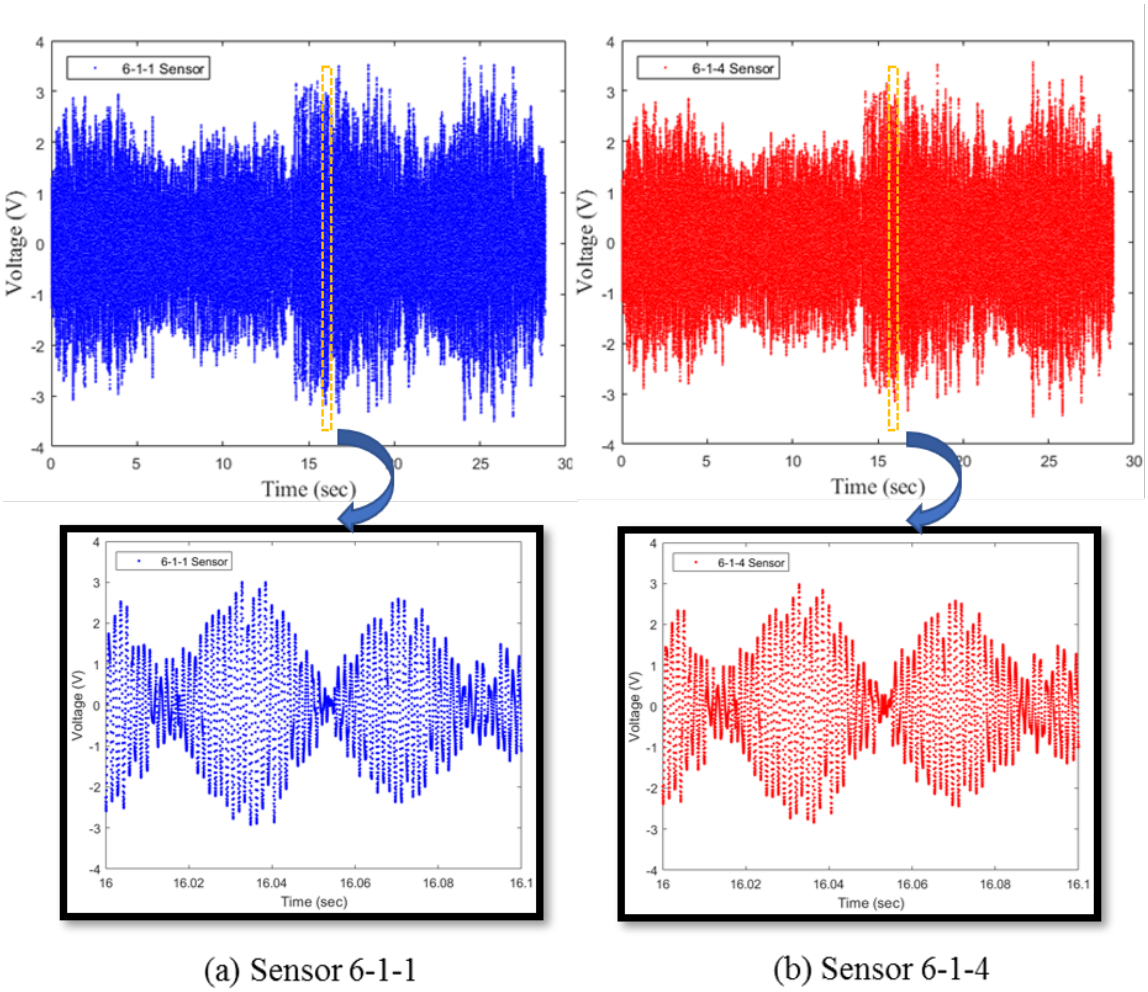

Thirty-second recording of a hovering Yuneek Typhoon UAV was played. The bottom figures are a magnification of the dashed areas on the corresponding top graphs.

Figure 22. Temporal response of the MEMS sensors to a recording of Yuneek Typhoon UAV sound.

Next, the sensors, arranged in canted angle with 15 degrees offset, were rotated from -75 to +75 degrees while the file with the Typhoon sound was played in a repeat mode. The sensors were held for ten seconds at every five-degree rotation. The recorded outputs correspond to a vector comprised of 33,000 elements, 1,000 elements per each five degrees, and 100 elements per second. This is plotted in Figure 23, and displayed separately to avoid confusing clutter. It is clear from the figure that a repetitive pattern, due to the repetition of the same file several times, can be identified. In addition, the

responses are almost identical except that the average minimum and average maximum are shifted by about 30 degrees, as would be expected.

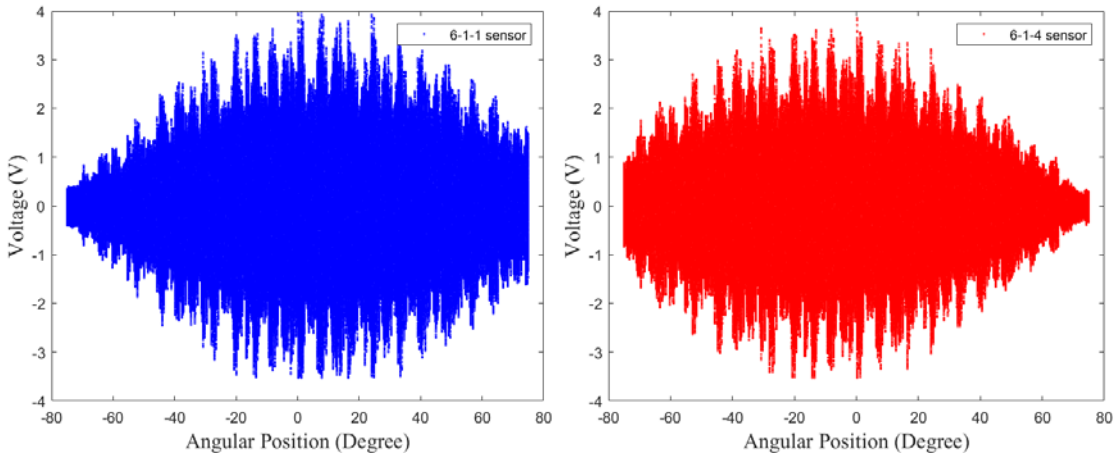

Arranged in canted angle with 15 degrees offset, measured by a DAS.

Figure 23. Directional response test of the MEMS directional sensors

Based on the measured results, a few approaches can be used to compute the direction of arrival. A thorough signal processing study and analysis is beyond the scope of this thesis. Instead, a simple algorithm is applied to prove the concept and prepare the ground for future work.

The data from both sensors were squared to provide a response similar to the theoretical curve shown in Figure 14. Then they were integrated (added) for time intervals, going from 1 to 10 seconds for each angle, according to the following equations.

$$\sum {V_L}^2 = \begin{pmatrix} for\ 0{\sim}1\ seconds, \sum_1^{100} {V_L}^2 \\ for\ 1{\sim}2\ seconds, \sum_{101}^{200} {V_L}^2 \\ \cdot \\ \cdot \\ \cdot \\ for\ 9{\sim}10\ seconds, \sum_{901}^{1000} {V_L}^2 \end{pmatrix} \quad (7)$$

$$\sum V_R^{\,2} = \begin{pmatrix} for\ 0{\sim}1\ seconds, \sum_1^{100} V_R^{\,2} \\ for\ 1{\sim}2\ seconds, \sum_{101}^{200} V_R^{\,2} \\ \cdot \\ \cdot \\ \cdot \\ for\ 9{\sim}10\ seconds, \sum_{901}^{1000} V_R^{\,2} \end{pmatrix} \tag{8}$$

This was done to provide insight on how the results will behave as we increase the integration time for each degree. It is worth mentioning that for non-cooperative small UAVs with dynamic integration times greater than three seconds, the accuracy of the measurement can be greatly compromised.

Finally, the DoA was calculated for all intervals as

$$\theta = tan^{-1}\left(\frac{1}{\tan(\theta_{off})} \times \frac{\sqrt{\sum V_L^{\,2}} - \sqrt{\sum V_R^{\,2}}}{\sqrt{\sum V_L^{\,2}} + \sqrt{\sum V_R^{\,2}}}\right)$$
$$for\ -90° + \theta_{off} \leq \theta \leq 90° - \theta_{off}. \tag{9}$$

The argument of the arctan in Equation (9) was plotted in Figure 24, for each measured angle, for several integration intervals. In the figure, the red solid lines represent the ideal theoretical value as if the sensors' responses were perfect cosines.

This preliminary result is very encouraging since no signal conditioning such as filtering, rectification, smoothing, etc., as well as no signal processing other than integration was applied. It is observable that there is no ambiguity in the range of detection and the output gets smoother as the integration time increases. It seems the three-second integration time gives a reasonably smooth response. The calculated differences over the sums show a small asymmetry that can be easily explained by misalignment of the normal incidence.

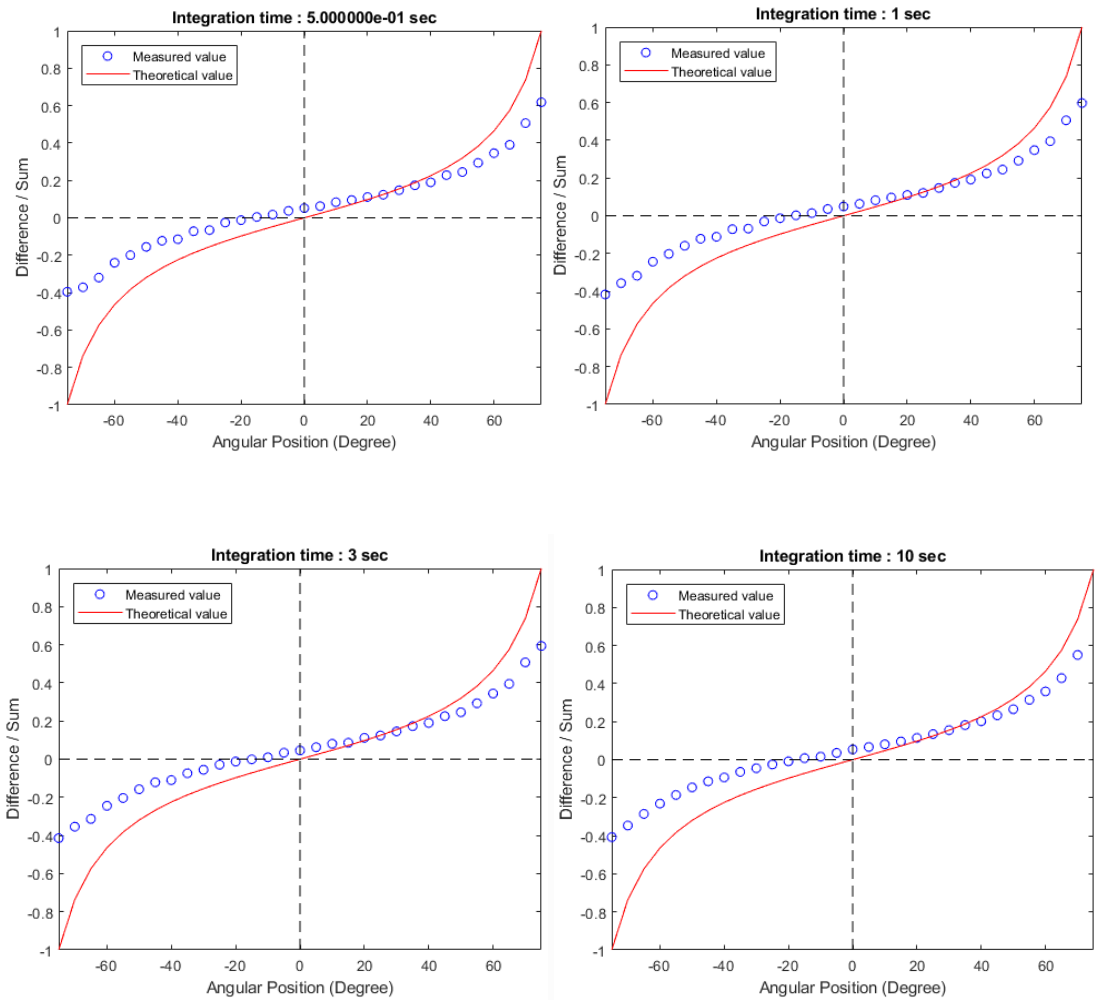

The integration time changed from 0.5, 1, 3, and 10 seconds.

Figure 24. Difference over the sum of the MEMS sensors' detection of the Typhoon sound.

For the sake of comparison, Figure 25 shows the detected angle calculated using Equation (9) plotted against the actual angle for the same integration intervals shown in Figure 24. The red solid lines indicate the ideal response.

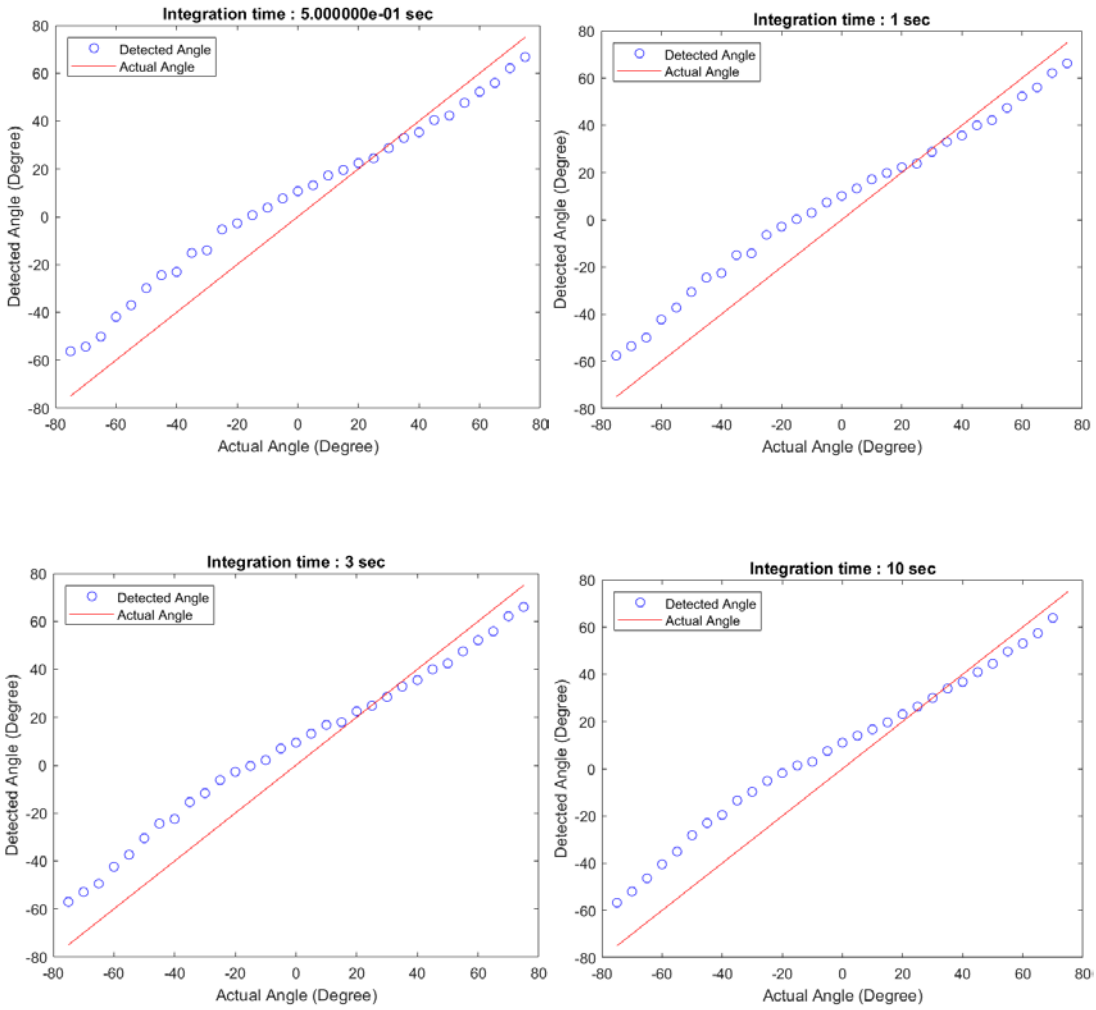

Figure 25. Comparison between detected and actual angle of arrival of the Typhoon sound.

The observed difference is up to 20 degrees, with an average of 11 degrees, again due to misalignment, interference of the mounting, wiring, and many other factors. Simple calibration methods such as fitting curves or lookup tables can be employed to compensate for those factors and provide an accurate response.

This result is significant since such detection has never been obtained before with co-located sensors having a total footprint of only about 5 cm. This proof-of-concept, performed with the Yuneek Typhoon, represents only the first step in the DoA determination of small multi-rotor UAVs, by acoustic detection, without the need of sensor arrays or distributed sensors. This study provides the results for detecting the

horizontal azimuth, however, by adding another sensor, canted in elevation, and shows a three-dimensional DoA could be detected.

VI. CONCLUSIONS

A. SUMMARY

Currently, several research efforts are being conducted in acoustic detection and localization of small multi-rotor UAVs. The common characteristic among all reported detection systems is the use of arrays of sensors lacking a small footprint. In addition, sophisticated algorithms and signal processing techniques are applied to provide rather limited results, indicating the problem under study is not simple. The work detailed in this thesis succeeded in demonstrating an unconventional method of small multi-rotor UAV acoustic localization without the need for arrays, which instead uses two colocated sensors with a footprint no larger than a quarter dollar.

The acoustic signature of a Yuneek Typhoon hexacopter was studied and several strong spectral lines were identified between 300 and 2000 Hz. Consequently, a MEMS sensor was designed with a frequency response to match one particular strong line around 700 Hz. The sensor sensitivity showed a resonant behavior with about 100 Hz bandwidth, which is enough to capture the jitter on the sound noise due to rotor speed variations necessary to keep the flight regime.

The MEMS sensors, which mimic the hearing system of the parasitic fly *Ormia Ochracea*, exhibited two dominant oscillatory modes, rocking and bending. Both oscillation modes depend on the direction of arrival of the acoustic source; however, for this study, the sensors were operated in bending mode due to its higher sensitivity. Since the bending mode exhibits directional ambiguity around normal incidence, two sensors were used in a canted configuration. By using the difference over the sum of the vibration amplitudes of both sides, this study demonstrated an unambiguous detection between -75 and 75 degrees.

Preliminary results show that the error between the measured and actual angle of arrival is up to 20 degrees, with an average of 11 degrees, which can be corrected with simple calibration processes. This opens the possibility for the localization of small

UAVs without the need for complex arrays of microphones or sophisticated signal processing schemes.

Some observations made during this study are worth highlighting. First, although this study was conducted using a particular small multi-rotor UAV, it can be inferred from the open literature [20–22], [24] that the acoustic spectral characteristics of similar small multi-rotor aircraft are comparable, with a good match in spectral lines in the lower frequency range (< 2000 Hz). This allows for the studied sensor configuration to be used indiscriminately for a large number of small multi-rotor UAVs. Second, the canted configuration used in this study imposed an offset angle of 15 degrees between normal incidence and the sensors azimuth. This limited the range of detection between -75 and 75 degrees. Smaller offset angles could be used to expand this range. Furthermore, the introduction of a third sensor could provide 360 degrees of coverage. Third, the MEMS sensors can be designed to exhibit multiple resonances (controlled spectral sensitivity) according to the acoustic signature of the multi-rotor aircraft. This would enhance the sensitivity while preserving the natural filtering of undesired frequency bands. Furthermore, by exploring the differences in signatures, it is possible to perform identification. Fourth, the acquired signals from the sensors were integrated (averaged) with different time intervals, and the integration showed that despite the increase in smoothness on the angular response, there is not much difference between 0.5- and 10-second integration times. Therefore, fast detection can be employed, which could be particularly interesting for tracking. Finally, unambiguous detection of the direction of arrival of the sound produced by a hovering small multi-rotor aircraft was successfully demonstrated. The scope of this work was limited to a proof-of-concept approach and many opportunities for future work can be identified.

B. RECOMMENDATIONS FOR FUTURE WORK

The immediate recommended follow-on work is the measurement of the DoA of different small UAVs. Also, instead of a recording, the experiment should be repeated with an actual aircraft hovering initially in the anechoic chamber, and then in open field

in the presence of background noise. Different flight regimes and loads should also be tried.

Another area to pursue would be the application of simple calibration algorithms, such as lookup tables or curve fitting. In addition to DoA estimation, the calibration process can be performed by an inexpensive microprocessor such as Arduino or Teensy. These microprocessors possess built-in fast analog-to-digital converters and high-speed processing capabilities that would allow for the DoA to be estimated in real time.

The use of distributed sensors, networked together, should be tested for precise localization through cross azimuth computation. Elevation could also be detected with a slightly different sensor configuration. This would also allow for tracking, which would be extremely valuable especially in close range where the countermeasures must be deployed.

On the sensor side, since the rocking motion is proportional to the sine of the angle of arrival, the use of a single sensor for unambiguous detection would be possible. Similar DoA determination algorithms can be used, considering the difference over the sum of the vibration amplitudes of both wings. In this case, an extremely small detection system could be made, especially if dedicated electronics can be integrated in the same die as the MEMS device.

THIS PAGE INTENTIONALLY LEFT BLANK

LIST OF REFERENCES

[1] A. Liptak, “The FAA says the commercial drone market could triple in size by 2023,” The Verge, May 4, 2019. [Online]. Available: https://www.theverge.com/2019/5/4/18529241/faa-annual-aviation-report-hobby-commercial-drones-prediction-2023

[2] L. Brown, “Drone applications at present and in the future,” Wondershare Filmora, May. 20, 2019. [Online]. Available: https://filmora.wondershare.com/drones/drone-applications-and-uses-in-future.html

[3] K. Wackwitz, “The drone applications report 2019,” Drone Industry Insights UG, Hamburg, Germany, Jan. 28, 2019. [Online]. Available: https://www.droneii.com/drone-applications-2019#1525106654181-a2b63cd6-e0c3

[4] P. Jeff, “Drone over White House highlights security concerns,” CBS News, Jan. 26, 2015. [Online]. Available: https://www.cbsnews.com/news/drone-over-white-house-sparks-new-security-concerns/

[5] C. Forrest, “17 drone disasters that show why the FAA hates drones,” Tech Republic, Jun. 13, 2018. [Online]. Available: https://www.techrepublic.com/article/12-drone-disasters-that-show-why-the-faa-hates-drones/

[6] C. Shalby, M. Puente, and H. Fry, “Illegal drones ground water-dropping helicopters at critical moment in fire battle,” *Los Angeles Times*, Nov. 2, 2019. [Online]. Available: https://www.latimes.com/california/story/2019-11-01/maria-fire-drone-hinders-firefighting-efforts-as-blaze-doubles-in-size-overnight

[7] P. McGreevy, “Private drones are putting firefighters in ‘immediate danger,’ California fire official says,” *Los Angeles Times*, Aug. 18, 2015. [Online]. Available: https://www.latimes.com/local/political/la-me-pc-fire-officials-warn-lawmakers-about-threat-of-drones-to-firefighting-aircraft-20150818-story.html

[8] D. Waldstein, “Drone crash interrupts match,” *New York Times*, Sep. 3, 2015. [Online]. Available: https://www.nytimes.com/live/us-open-results/drone-crash-interrupts-match/

[9] M. Grez, “Drone crashes onto piste, misses champion skier by inches,” CNN, Dec. 23, 2015. [Online]. Available: https://goo.gl/jtPdLh

[10] “Gatwick Airport drone incident,” *Wikipedia*. Accessed Jul. 1, 2020. [Online]. Available: https://en.wikipedia.org/wiki/Gatwick_Airport_drone_incident

[11] B. John, “US Army selects Raytheon for near-term counter-UAS mission,” Raytheon Company, Waltham, MA, USA, Jul. 17, 2018.

[12] O. Tom, “North Korea is invading South with spy drones, but they keep crashing,” *Newsweek*, Jun. 21, 2017. [Online]. Available: https://www.newsweek.com/north-korea-spy-us-missiles-consequences-south-628045

[13] M. Laura, “North Korea ‘has HUNDREDS of biochemical attack drones’ as fears of global war soar,” *Express*, May 24, 2017. [Online]. Available: https://www.express.co.uk/news/world/808658/North-Korea-drones-Donald-Trump-South-Korea-strike-missiles-WW3

[14] C. Gabriel, C. John, and K. Matthew, “UAS detection, classification, and neutralization: Market survey 2015,” Sandia National Laboratories, Livermore, CA, USA, 2015.

[15] S. R. Ganti and Y. Kim, “Implementation of detection and tracking mechanism for small UAS,” presented at the 2016 International Conference on Unmanned Aircraft Systems (ICUAS), Arlington, VA, 2016.

[16] J. Garcia-Gomez et al., “Cost-constrained drone presence detection through smart sound processing,” in *Proceedings of the 8th International Conference on Pattern Recognition Applications and Methods*, 2019. [Online]. doi:10.5220/0007556007660772.

[17] D. Wilmott, F. Alves, and G. Karunasiri, “Bio-inspired miniature direction finding acoustic sensor,” *Scientific Reports*, vol. 6, pp. 29975, 2016.

[18] J. O. Mutton, “Acoustic ground sensors to triangulate bomb impact in support of airfield damage assessment,” M.S. thesis, Dept. of Computer Science, NPS, Monterey, CA, USA, 2019. [Online]. Available: http://hdl.handle.net/10945/62813

[19] Grind Drone, “List of 40 applications for drones,” Aug. 26, 2017. [Online]. Available: http://grinddrone.com/applications/40-drone-applications-list

[20] J. A. Feight, S. Whyte, J. D. Jacob, and R. J. Gaeta, “Acoustic characterization of a multi-rotor UAs as a first step towards noise reduction,” in *55th AIAA Aerospace Sciences Meeting*, 2017, p. 1174.

[21] T. Zhou, H. Jiang, Y. Sun, R. J. Fattah, X. Zhang, B. Huang, and L. Cheng, “Acoustic characteristics of a quad-copter under realistic flight conditions,” in *25th AIAA/CEAS Aeroacoustics Conference*, 2017, p. 2587.

[22] N. Kloet, S. Watkins, and R. Clothier, “Acoustic signature measurement of small multi-rotor unmanned aircraft systems,” *International Journal of Micro Air Vehicles*, vol. 9, no. 1, pp. 3–14, Mar. 1, 2017.

[23] A. Bernardini et al. “Drone detection by acoustic signature identification,” *Society for Imaging Science and Technology*, Springfield, VA, USA. [Online]. doihttps://doi.org/10.2352/ISSN.2470-1173.2017.10.IMAWM-168

[24] A. G. Fleming, “Feasibility of detecting and classifying small unmanned aerial system threats using acoustic data,” M.S. thesis, Systems Engineering Dept., NPS, Monterey, CA, 2019. [Online]. Available: http://hdl.handle.net/10945/64157

[25] T. Pham, and L. Sim, “Acoustic detection and tracking of small, low-flying threat aircraft,” in *23rd Army Science Conference*, Dec. 2002. [Online] Available: https://www.semanticscholar.org/search?q=Acoustic%20detection%20and%20tracking%20of%20small%2C%20low-flying%20threat%20aircraft&sort=relevance

[26] I. J. Jung, and J. G. Ih, “Acoustic localization and tracking of the multiple drones,” In *INTER-NOISE and NOISE-CON Congress and Conference Proceedings*, Institute of Noise Control Engineering, vol. 259, no. 8, Sep. 2019, pp. 1373–1377.

[27] A. Hommes et al. “Detection of acoustic, electro-optical and RADAR signatures of small unmanned aerial vehicles,” in *Proceedings of SPIE 9997, Target and Background Signatures II*, 999701, Oct. 24, 2016. [Online]. doi: 10.1117/12.2242180

[28] Z. Yingzhe, L. Incheol, and L. Dakai, “Measurement of noise from a moving drone using a phased array microphone system,” in *2017 Asia-Pacific International Symposium on Aerospace Technology*, Seoul, Korea, Oct. 2017. [Online] Available: https://www.researchgate.net/publication/326697206

[29] T. Blanchard, J. Thomas, and K. Raoof, “Acoustic localization estimation of an unmanned aerial vehicle using microphone array,” presented at Inter Noise 2019, Madrid, Spain, Jun. 16–19, 2019.

[30] F. Alves, private communication, Jun. 2020.

[31] K. S. Brentner and F. Farassat, “Modeling aerodynamically generated sound of helicopter rotors,” *Progress in Aerospace Sciences*, vol. 39, pp. 83–120, 2003.

[32] A. A. Espinoza Peyrot, *Packaging and Characterization of Bio-inspired Underwater MEMS Directional Sound Sensor*, 2019. [Online Video]. Available: https://calhoun.nps.edu/handle/10945/62596.

[33] R. C. Rabelo, F. D. Alves, and G. Karunasiri, “Electronic phase shift measurement for the determination of acoustic wave DOA using single MEMS biomimetic sensor,” *Scientific Reports*, vol. 10, no. 1, pp. 1–13, 2020.

[34] MEMSCAP: SOIMUMPs and MEMS Multi Project Wafer Service. (n.d.). MEMSCAP. Accessed Jul. 17, 2020. [Online]. Available at: http://www.memscap.com/ products/mumps/soimumps/

[35] M. L. Kuntzman, N. N. Hewa-Kasakarage, A. Rocha, D. Kim, and N. A. Hall, “Micromachined in-plane pressure-gradient piezoelectric microphones,” *IEEE Sensors Journal*, vol. 15, no. 3, pp. 1347–1357, 2014.

INITIAL DISTRIBUTION LIST

1. Defense Technical Information Center
   Ft. Belvoir, Virginia

2. Dudley Knox Library
   Naval Postgraduate School
   Monterey, California